Fall 12-20-2013

A Study on the Integration of a Novel Absorption Chiller into a Microscale Combined Cooling, Heating, and Power (Micro-CCHP) System

Scott J. Richard
sjrichar@uno.edu

A Study on the Integration of a Novel Absorption Chiller into a Microscale Combined Cooling, Heating, and Power (Micro-CCHP) System

A Thesis

Submitted to the Graduate Faculty of the
University of New Orleans
in partial fulfillment of the
requirements for the degree of

Master of Science
in
Engineering
Mechanical Engineering

by

Scott J. Richard

B.S. University of New Orleans, 2011

December, 2013

ACKNOWLEDGEMENT

I would like to express my heartfelt gratitude to Dr. Ting Wang, whose dedication to his students is paralleled only by his enthusiasm for understanding the physical world in a deep and practical way. Without his patient guidance, I would not be the engineer I am today.

I would like to thank all of my friends and colleagues in the Energy Conversion and Conservation Center research group who have helped me on my journey to obtaining my Masters degree.

I would like to acknowledge the Opportunities for Partnerships in Technology with Industry (Opt-In) program supported by the Board of Regents, as well as Aestus Power, for facilitating this research.

I would like to thank my brother, Patrick, who has demonstrated the value of sound work ethic and self-discipline through his personal academic achievements.

I would like to thank my parents, John and Pam, who stopped at nothing to provide me with the highest quality education available.

Finally, I would like to acknowledge my wife and best friend, Jen, whose steadfast love and support has given me the courage to pursue my passion for engineering.

TABLE OF CONTENTS

LIST OF FIGURES

LIST OF TABLES

NOMENCLATURE

ACS	Absorption chiller system
BCHP	Building cooling, heating, and power
CCHP	Combined cooling heating and power
CHP	Combined heating and power
COP	Coefficient of performance
DG	Distributed generation
EES	Engineering Equation Solver
HHV	Higher heating value
HRSG	Heat recovery steam generator
HRU	Heat recovery unit
HX	Heat exchanger
LHV	Lower heating value
LiBr	Lithium bromide
m_i	State point mass flow rate (kg/s)
MGT	Micro Gas Turbine
P_i	State point pressure
Q_a	Net rate of heat transfer from absorber (kW)
Q_c	Net rate of heat transfer from condenser (kW)
Q_{cg}	Net rate of heat transferred internally from high condenser to low generator (kW)
Q_e	Net rate of heat transfer into evaporator (kW)
Q_g	Net rate of heat transfer into generator (kW)
Q_{hw}	Net rate of heat transfer from microturbine exhaust to hot water stream
q_i	State point vapor quality
RT	Refrigeration Ton
T_i	State point temperature
x	Mass fraction (%)

ABSTRACT

This study explores the application of micro-CCHP systems that utilize a 30 kW gas microturbine and an absorption chiller. Engineering Equation Solver (EES) is used to model a novel single-effect and double-effect water-lithium bromide absorption chiller that integrates the heat recovery unit and cooling tower of a conventional CCHP system into the chiller's design, reducing the cost and footprint of the system. The results of the EES model are used to perform heat and material balances for the micro-CCHP systems employing the novel integrated chillers, and energy budgets for these systems are developed. While the thermal performance of existing CCHP systems range from 50-70%, the resulting thermal performance of the new systems in this study can double those previously documented. The size of the new system can be significantly reduced to less than one third the size of the existing system.

Keywords: Micro-CCHP, absorption chiller, cogeneration, EES, computational, lithium bromide

CHAPTER 1

MICRO-COMBINED COOLING, HEATING, AND POWER OVERVIEW

1.1 Introduction to Combined Cooling, Heating, and Power

Cogeneration, or Combined Heating and Power (CHP), is the simultaneous production of electrical and thermal energy for process or space heating from a single fuel source, which is converted from chemical energy to mechanical energy by a prime mover—internal combustion engine, gas turbine, fuel cell, among others. In combined cooling, heating, and power (CCHP), also commonly referred to as polygeneration or trigeneration, a single fuel source produces electrical energy and thermal energy and adds space cooling or chilled water to the useful products of a CHP system.

The production of multiple useful energy products by a single fuel source is accomplished by capturing the energy present in the prime mover's exhaust gas. This energy, or waste heat, that would otherwise be dissipated in the surroundings is instead harnessed by various means and is used to produce heating and/or cooling without using additional fuel. For example, a gas turbine with a thermal efficiency of 26% produces—at ideal conditions—26 kW of electrical energy for every 100 kW of fuel input. A small portion of the 100 kW is lost as radiation and convective heat losses through engine surfaces, leaving close to 71 kW of waste heat in the turbine's exhaust. The majority of this waste heat can be captured and used, for instance, to heat a process stream that would otherwise require a dedicated boiler and a separate fuel source to heat it. The waste heat can also be used to drive a cycle in a thermally-activated machine, a device such as an absorption chiller, adsorption chiller, an organic Rankine cycle, or a dessicant dehumidifier, that is powered by a thermal input rather than an electrical input.

Polygeneration systems exist in a wide range of capacities from 1 kW to over 1 GW. The research contained herein focuses on micro-combined cooling, heating, and power (micro-CCHP) located nearby the user. Many definitions of what constitutes a "micro-scale"

polygeneration system can be found in the literature on such systems (Angrisani, Roselli & Sasso, 2012); however, the definition of micro-CCHP systems used in this report applies to those systems having an **electrical power** generation capacity of **100 kW** or less.

1.2 Benefits of CCHP

There are many advantages to on-site polygeneration systems, or Distributed Generation (DG), that make them appealing for different applications when compared to conventional power generation systems, like a centralized power plant. Some of these advantages are the following:

- DG systems have low total capital cost (not necessarily $/kW).
- It is convenient and fast to add incremental power to a DG system.
- DG significantly reduces transmission and distribution (T&D) costs.
- DG minimizes T&D line losses.
- DG systems provide a standalone power option for areas with no T&D infrastructure.
- DG systems provide a more flexible and efficient means of employing CHP or CCHP.
- DG provides a self-generating capability during high-cost peak-load periods.

1.3 CCHP Applications

Combined cooling, heating, and power can be used in a wide variety of applications. Theoretically, a CCHP configuration can be applied wherever there is a prime mover that generates waste heat. In practice, certain industries lend themselves better to CCHP systems than others. Combined cooling, heating, and power systems have found a niche in buildings so much so that a separate term—Building Cooling, Heating, and Power (BCHP)—has been coined to describe CCHP systems employed in a building (Yin, 2006). Smaller office buildings or apartment complexes can employ a micro-CCHP system for power generation, production of cold water to meet space-cooling needs in the summer, and production of hot water for heating needs in the colder months. Larger buildings, like hotels or hospitals, can use a large-scale CCHP system for similar purposes, especially utilizing hot water production to launder linens instead of expending additional fuel to heat the water. The BP Helios Plaza, a 400,000

square foot office building in Houston, Texas, has a 4.3 MW CCHP system using a combustion turbine with turbine inlet cooling, a heat recovery steam generator (HRSG), an absorption chiller, and a chilled water storage tank to provide 100% of the buildings energy and chilled water needs (U.S. DOE Gulf Coast Clean Energy Application Center).

Agriculture is another industry well-suited for CCHP applications. In underdeveloped rural areas lacking an electric power infrastructure, an on-site CCHP system may be the best option for generating power and refrigeration to preserve valuable crops before the product can be transported to the market. Refineries, where processes produce or require heat, also utilize CCHP systems to reduce fuel consumption in boilers to heat process fluids. For example, Targa Resources has a natural gas liquid fractionation refinery in Mont Belvieu, Texas, with a 15.0 MW CHP system. The system, which uses a gas turbine to meet 70-90% of the facilities electricity needs, has a thermal efficiency of 90% and produces approximately 260,000 lbs/hr of steam using a duct-fired HRSG (U.S. DOE Gulf Coast Clean Energy Application Center). These are just a few examples of industries that use CCHP systems. As the government releases tax incentives for CCHP users and the benefits of these systems become more well-established, more industries are finding ways to convert from their current power generation means to CCHP.

1.4 Micro-CCHP System Components

A typical micro-combined cooling, heating, and power system consists of a prime mover, such as a reciprocating engine or a gas turbine; a heat recovery unit to capture the waste heat from the prime mover; a thermally activated device, such as an absorption chiller; and a cooling tower. Figure 1.1 shows the components of a typical micro-CCHP system. The prime mover in Figure 1.1 is a gas turbine, which produces electricity when coupled to a generator. The exhaust gas from the turbine is captured by the heat recovery unit (HRU), which uses a portion of the exhaust gas energy to produce hot water to be utilized as needed by the user. That portion of the turbine exhaust energy that is not used to produce hot water or is not irreversibly lost to the surroundings is passed on to the absorption chiller, which uses the exhaust energy to drive the absorption cycle rejecting heat to a cooling tower and producing chilled water for

refrigeration, space cooling, or other cold water needs. If the chilling capacity is more important than hot water instead, the waste heat will be first used to generate chilling water. The absorption cycle will be discussed in more detail in Chapter 2.

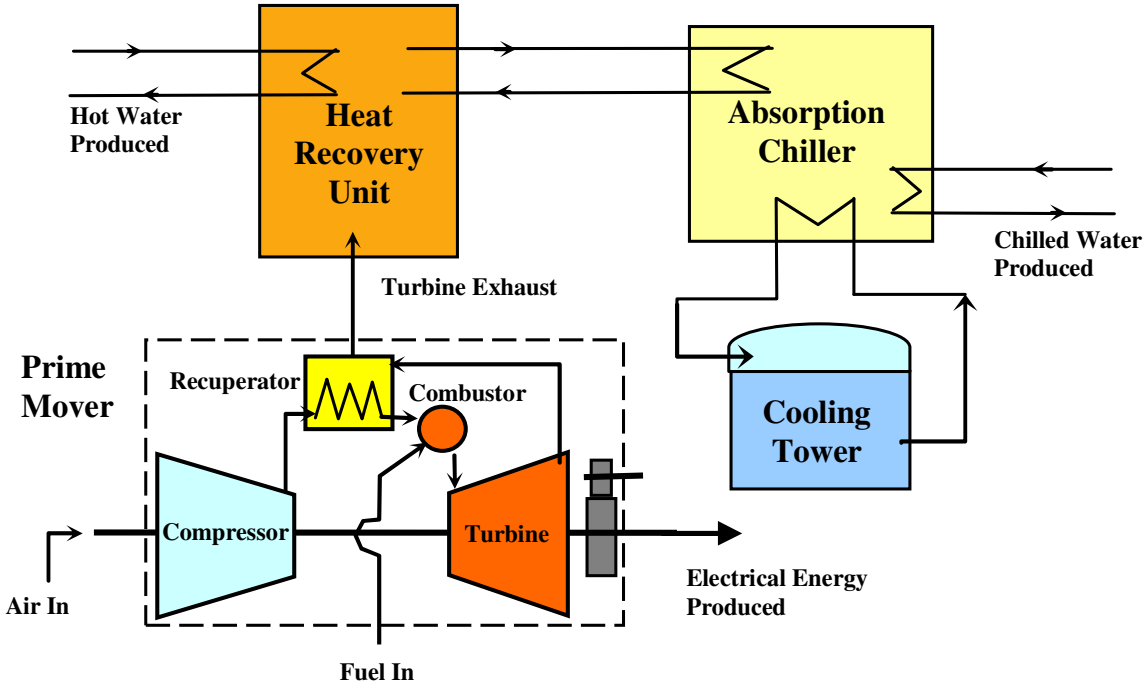

Figure 1.1 A typical micro-CCHP system configuration

1.4.1 Micro-CCHP Prime Movers

The two most common prime movers used in micro-CCHP applications are reciprocating engines and gas turbines. Both of these prime movers achieve the same effect: the conversion of chemical energy to mechanical energy, which is used to drive a generator to produce electrical energy. However, they achieve this conversion in very different ways.

1.4.1.1 Reciprocating Engines

With thermal efficiencies ranging from 20-40%, reciprocating internal combustion engines are the most commonly used prime movers in micro-CCHP systems. Waste heat from a reciprocating engine can be recovered most readily from engine exhaust gases and engine jacket coolant by means of a heat exchanger, as shown in Figure 1.2. There are two types of

reciprocating engines used in micro-CCHP applications: spark ignition (SI) engines and compression ignition (CI) engines.

Spark ignition engines can use many different kinds of fuel, but a very common fuel in micro-CCHP applications is natural gas. In a spark ignition engine, the fuel-air mixture is compressed in a cylinder. A spark ignites the mixture, which releases the chemical energy of the mixture. The chemical energy of the fuel is converted to mechanical energy when the gas in the cylinder expands, pushing the piston up and causing the crankshaft to rotate. The rotation of the crankshaft, when coupled to a generator, results in the generation of electrical energy.

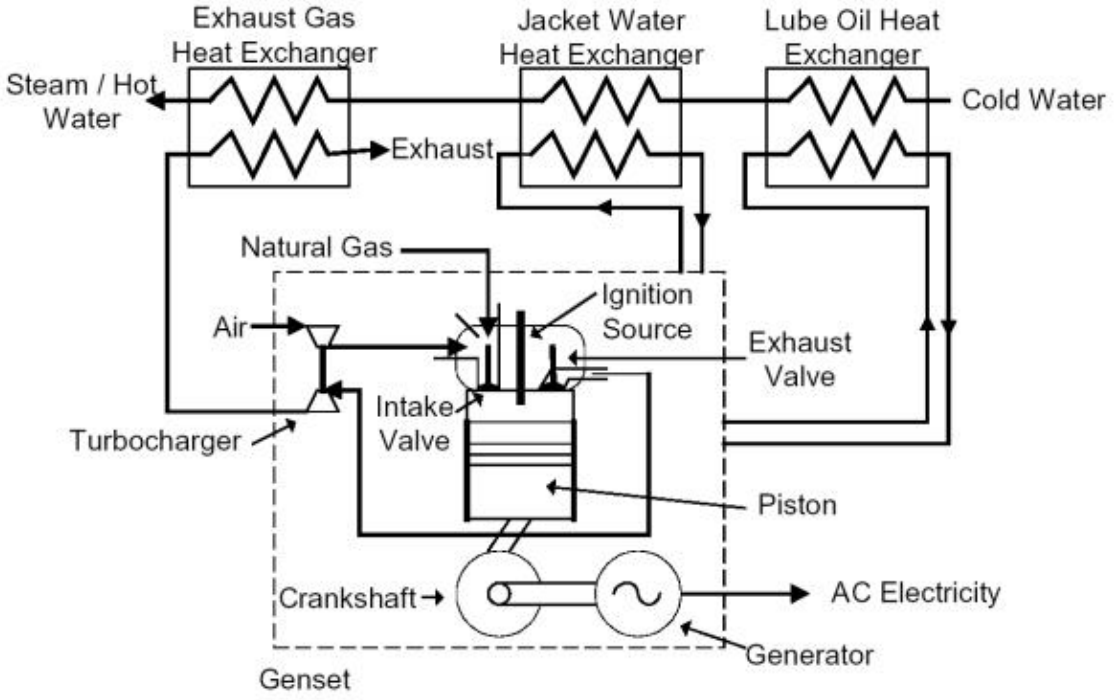

Figure 1.2 An example of reciprocating engine waste heat recovery (Source: Energy Solutions Center, Inc., 2012)

The second type of reciprocating engine used in micro-CCHP systems is the compression ignition engine, which is most commonly powered by diesel fuel. As opposed to a spark ignition engine in which the fuel and air are both compressed in the cylinder, in a compression ignition engine, only the air is compressed in the cylinder. During the compression process, the air in the cylinder heats up enough to provide an adequate temperature for the combustion of fuel to

occur. Near the end of compression, the fuel is injected into the cylinder and combusts in the hot cylinder. As with the spark ignition engine, the combustion of the fuel-air mix causes the mix to expand and push the piston out, rotating the crankshaft connected to the electrical generator. In a compression ignition engine, the air in the cylinder undergoes more compression than the fuel-air mix in a spark ignition engine. Because of this higher compression ratio, compression ignition engines have higher efficiencies than SI engines and are often the reciprocating engine of choice in micro-CCHP systems. Usually, the efficiency of smaller reciprocating engines is less than 30%.

1.4.1.1.1 Advantages and Disadvantages of Reciprocating Engines

There are advantages and disadvantages to utilizing a reciprocating engine as the prime mover in a micro-CCHP system. The following are the advantages of reciprocating engines as prime movers (Wu & Wang, 2006):

- Reciprocating engines are available in a wide range of sizes to meet the requirements of a polygeneration system.
- Reciprocating engines require the lowest initial capital cost when compared to other prime movers.
- Reciprocating engines have the fastest start up time.
- Reciprocating engines have high efficiencies at part load operation.

The disadvantages of reciprocating engines as prime movers are the following (Uzuneanu & Scarpete, 2011):

- Reciprocating engines are the noisiest prime movers.
- Reciprocating engines are the largest in size and have the greatest weight.
- Reciprocating engines require more maintenance than other prime movers.
- Reciprocating engines have higher emission levels than other prime movers.

Finally, another disadvantage of reciprocating engines is that the temperatures of their exhaust gas and jacket cooling water are too low for CCHP.

1.4.1.2 Gas Microturbines

A gas microturbine, as shown in Figure 1.3, is defined as a gas turbine with an electric power output capacity of 300 kW or less. Microturbines are based on technology originally developed for aircraft propulsion. Like reciprocating engines, microturbines convert the chemical energy of a fuel into mechanical energy, which is further converted into electrical energy; but the means by which they accomplish this conversion is very different from reciprocating engines. First, air is drawn into and compressed in the compressor. Next, fuel is injected into the compressed airstream, and the fuel-air mix is ignited in the combustor. The combustion of the fuel-air mix causes it to expand. The expansion process of the hot, high pressure gases occurs through the turbine, where it causes several rows of blades connected to a shaft to rotate. The turbine shaft is coupled to a generator, which converts the mechanical energy of the turbine's shaft rotation into electrical energy. As with reciprocating engines, waste heat can be recovered from the exhaust gases of the microturbine via a heat exchanger. The overall efficiency of a conventional micro-CCHP system with a microturbine prime mover is close to 80% (Uzuneanu & Scarpete, 2011).

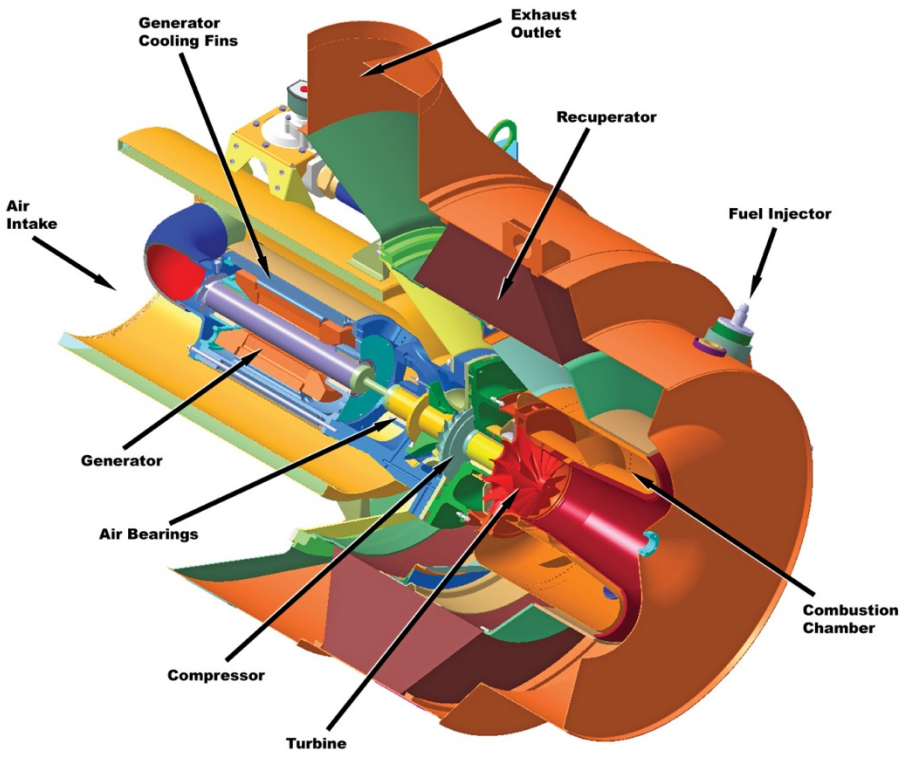

Figure 1.3 Cutaway of 30 kW Capstone microturbine (Source: Capstone Turbine Corporation, 2012)

1.4.1.2.1 Advantages and Disadvantages of Gas Microturbines

There are advantages and disadvantages to utilizing a gas microturbine as the prime mover in a micro-CCHP system. The following are the advantages of microturbines as prime movers (Uzuneanu & Scarpete, 2011):

- Microturbines are small and lightweight. This makes them a competitive prime mover option in packaged micro-CCHP systems or where space and weight are restricted.
- Microturbines have lower emissions than reciprocating engines.
- Because there is only one moving part, less maintenance is required for a microturbine than for a reciprocating engine.
- Microturbines can be easily combined into large systems with multiple units.
- The exhaust temperature is higher than reciprocating engines and is, therefore, more efficient for implementing CHP.

The disadvantages of microturbines as prime movers are the following:

- Microturbines have a higher capital cost than reciprocating engines.
- Microturbines have a shorter life cycle—10 years—than reciprocating engines, which have an average life cycle of 20 years.
- Microturbines have a lower efficiency than reciprocating engines.
- The part load operating performance of a microturbine is poor compared to that of a reciprocating engine.
- The performance of microturbines is more sensitive to fluctuations in ambient conditions.

1.4.2 Heat Recovery Units

There are many devices that can be used to capture exhaust gas waste heat from a prime mover. One means of recovering energy from an engine exhaust stream is to use a shell and tube heat exchanger to transfer heat from the hot exhaust gas to water circulating in the

exchanger tubes. The hot tube side water can then be used to provide the thermal input for a thermally activated machine and/or a portion of it can be used directly to fulfill the hot water needs of the application. Another means of capturing waste heat is to use an exhaust steam generator with or without forced circulation provided by a blower—depending on the pressure of the engine exhaust gas—to transfer heat from the exhaust gas to water flowing in a coil of finned tubes. Figure 1.4 depicts engine exhaust waste heat recovery with an exhaust steam generator.

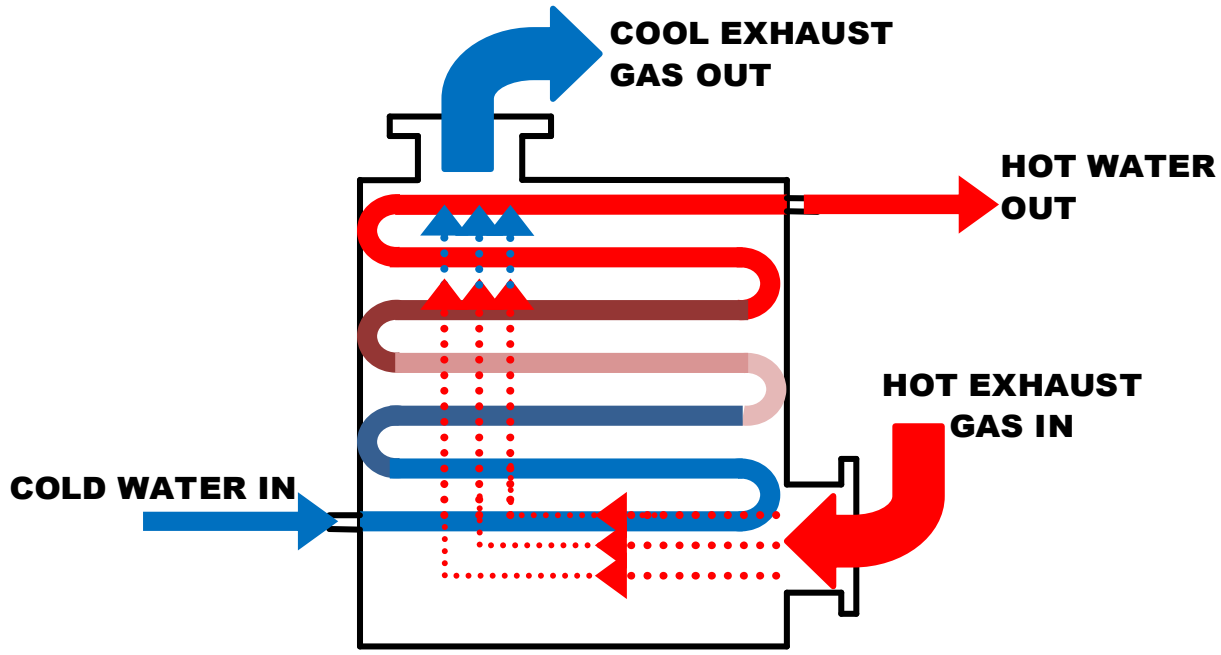

Figure 1.4 Coiled tube heat recovery unit

1.4.3 Absorption Chillers

Absorption chillers are thermally activated devices that use a heat input to drive a refrigeration cycle. Figure 1.5 depicts a single-effect absorption chiller. An absorption chiller can be easily understood by comparing it to a conventional vapor compression chiller. In a conventional vapor compression refrigeration cycle, heat is transferred from a low temperature reservoir to an evaporator and is rejected to a higher temperature reservoir from a condenser by means of a work input. In conventional vapor compression, the work input to the system comes from an electrical input to the compressor. In an absorption chiller, the compressor is

replaced by an absorption cycle, which is represented in Figure 1.5 by the components enveloped by the dotted line. The electrical input to the compressor of a conventional vapor compression system is replaced here by a thermal input to the generator in the absorption loop of the absorption chiller.

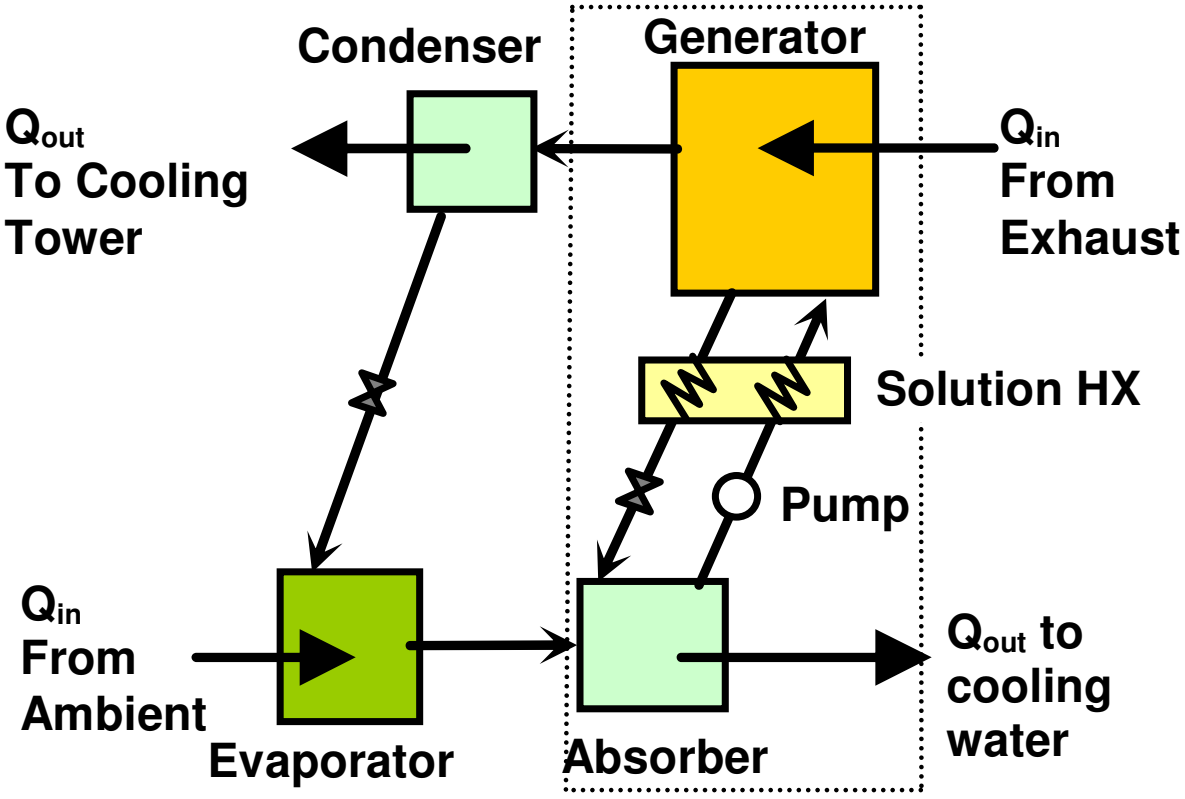

Figure 1.5 Single-effect absorption chiller

While a conventional vapor compression cycle uses one working fluid, an absorption chiller cycle makes use of two working fluids: an absorbent-refrigerant pair. The absorbent circulates in solution through the absorber-generator absorption loop of the absorption chiller, and the refrigerant circulates through the entire system. The thermal load that drives the cycle is input to the generator in the absorption loop. The heat input to the generator causes refrigerant in the absorbent-refrigerant solution to vaporize out of the solution, and it flows into the refrigerant loop of the absorption chiller, where it rejects heat from the condenser, undergoes a reduction in pressure through an expansion valve, and absorbs heat from the ambient in the evaporator. The refrigerant vapor flows from the evaporator into the absorber,

where it exothermically reacts with the absorbent causing the absorbent to dissolve into solution with it. This dilute solution is pumped through the solution heat exchanger, where it is pre-heated by the strong solution exiting the generator, and flows into the generator, where the driving heat input to the system vaporizes refrigerant out of it. The net effect of this cycle, as with conventional vapor compression, is to provide space cooling or refrigeration. Absorption chiller theory will be explored in more detail as the primary topic of Chapter 2, followed by a computational study of absorption chillers in Chapter 3.

1.5 Objectives

The purpose of this project is to explore the theory behind and feasibility of a pre-packaged micro-CCHP system consisting of only a gas microturbine and absorption chiller. The system aims to improve upon conventional packaged micro-CCHP systems by eliminating the heat recovery unit and cooling tower and thus reducing cost and footprint. Furthermore, the micro-CCHP system of this project seeks to achieve total system thermal performances doubling those of existing systems. The specific goals of this project are the following:

1. Conduct literature research into the theory of absorption chiller technology and its integration into micro-CCHP systems.

2. Develop and conduct a computational study of different absorption chiller configurations using Engineering Equation Solver software.

3. Investigate different options to integrate micro-CCHP system for reducing overall size but significantly improving performance.

4. Conduct overall energy balance for the integrated systems.

CHAPTER 2

ABSORPTION CHILLER FUNDAMENTALS

According to the Clausius Statement of the second law of thermodynamics, “It is impossible to construct a device that operates in a cycle and whose sole effect is the transfer of heat from a cooler body to a hotter body.” In order to transfer heat from a cooler body to a hotter body, typically work must be input to the system. This is exhibited in a conventional vapor compression chiller, in which an electric input drives a compressor that performs work on a working fluid, elevating its pressure in the process. Similar to a conventional vapor compression chiller, an absorption chiller is a machine that transfers heat from a low temperature reservoir to a higher temperature reservoir; however, instead of accomplishing this transfer of heat with an input of work, an input of thermal energy drives the cycle. The product of the cycle is a cooling load via, for example, chilled water or cooling air. By operating on a thermal input, an absorption chiller is well-suited for combined cooling, heating, and power applications where a source of waste heat is available. The fundamental theory and working principles of absorption chiller technology are the topic of this present chapter.

2.1 The Absorption Chiller: Thermally Activated Technology

The question may arise as to how it is possible to replace a work input with a heat input, as in absorption chillers, in transferring heat from a low temperature to a high temperature. The answer to this question can be obtained by comparing the absorption chiller cycle to the conventional vapor compression cycle. Section 1.3.3 in Chapter 1 presents a cursory overview of the absorption chiller cycle in comparison to the conventional vapor compression cycle. Figure 2.1 furthers this comparison graphically. The compressor in a conventional vapor compression chiller (Fig. 2.1c) is replaced, in an absorption chiller (Fig. 2.1a), by the components in the solution loop between state points 3 and 4—primarily, the absorber, generator, and solution pump. In the conventional vapor compression cycle, the net effect of the compressor, as shown on the T-s diagram of Figure 2.1b, is to increase the pressure and the temperature of the working fluid. It does so by means of a mechanical compressor that is powered by an electrical input. In an absorption chiller, the net effect of the solution loop on

the refrigerant is the same as that of the compressor on the working fluid in a conventional vapor compression chiller: to increase the pressure and temperature of the refrigerant. However, in an absorption chiller, the refrigerant's increase in pressure and its increase in temperature are accomplished by the solution pump and the heat input to the generator, respectively. The electrical energy required to run the solution pump can be as low as only 0.001-0.01% of the thermal energy input to the generator; therefore, the solution pump work is considered negligible, and an absorption chiller is classified as "thermally activated," or "heat-driven," technology. An absorption chiller may be direct-fired—combustion of a fuel source provides a direct heat input to the chiller's generator; or the chiller may be indirect-fired—the required heat input to the generator is provided by hot water, which is heated by an energy source such as waste steam or exhaust gas. Some unconventional absorption chillers make use of geothermal energy or solar radiation to drive the cycle.

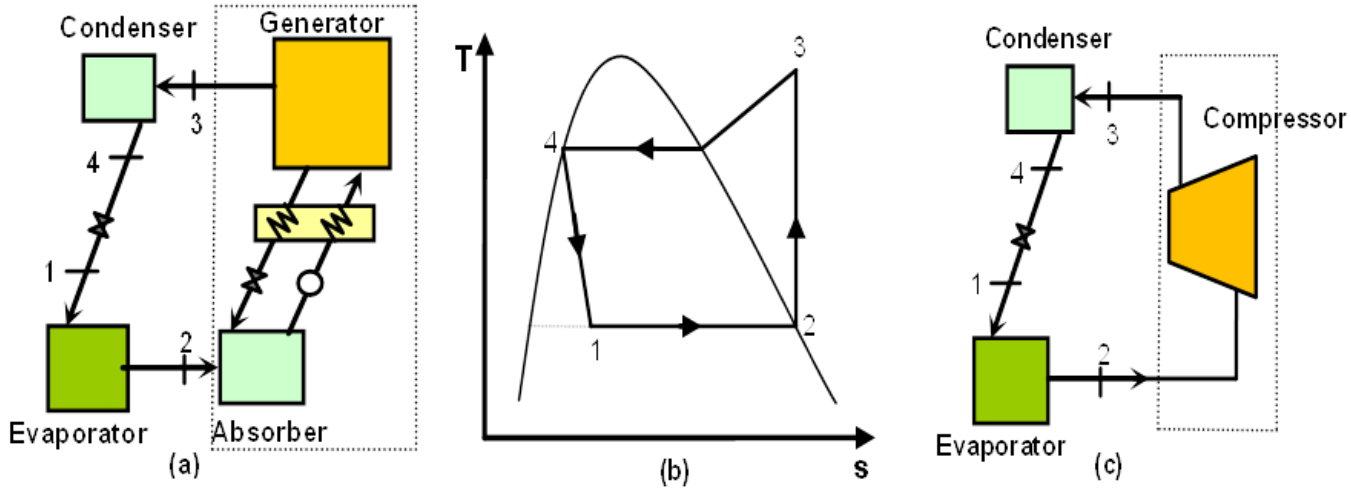

Figure 2.1 (a)Single-effect absorption chiller cycle; (b)T-s diagram qualitatively representing the net effect of the cycles; (c)Conventional vapor compression chiller cycle

2.2 Absorption Chiller Working Fluids

While a conventional vapor compression chiller uses a single working fluid, an absorption chiller utilizes a refrigerant-absorbent working fluid pair. The refrigerant circulates throughout the entire absorption chiller, while the absorbent circulates only through the solution loop inside the dotted box in Figure 2.1a. The following are some of the properties of

working fluid pairs that make them suitable for absorption chiller applications: the absence of a solid phase in the chiller's operating range; the absorbent should have a high affinity for the refrigerant; the absorbent volatility should be low relative to the refrigerant's so that the two can be easily separated in the generator (ASHRAE Handbook 2001 Fundamentals). Many different refrigerant-absorbent working fluid pairs are discussed in absorption chiller literature (Wang & Chua, 2009; Dorgan, Leight & Dorgan, 1995), but the two most commonly used are water/lithium bromide and ammonia/water.

2.2.1 Water-Lithium Bromide Absorption Chillers

The chiller of choice in this research project, water-lithium bromide (LiBr) chillers are a mature absorption chiller technology. They are available in sizes ranging from 5-1660 Refrigeration Tons (RT) (ASHRAE Handbook 2010 Refrigeration). They are reliable machines that have coefficients of performance (COP), the ratio of the evaporator's cooling output to the generator's heat input, ranging from 0.7-1.3 depending on the configuration of the chiller. As a working fluid pair, water-lithium bromide exhibits several desirable characteristics that make it well-suited for absorption chiller applications. One characteristic that makes water a good choice for an absorption chiller refrigerant is that it has a high latent heat (2260 kJ/kg); therefore, the refrigerant flow rate can be kept to a minimum, which allows for a reduction in the size of the chiller. Another desirable property of water as a refrigerant is that it has a low viscosity, which enhances mass and heat transfer and reduces the work of the solution pump. One characteristic of lithium bromide that makes it a good choice for an absorbent is that, like water, it also has a low viscosity. Moreover, lithium bromide's vapor pressure is very low compared to water's. For this reason, water can be easily vaporized out of solution in the generator without carrying lithium bromide with it. One limitation of water-lithium bromide chillers is that refrigeration temperatures must be maintained above 0°C, water's freezing point at standard conditions, to prevent icing in the evaporator.

2.2.2 Ammonia-Water Absorption Chillers

Ammonia-water absorption chillers are available in capacities ranging from 2-1000 RT and typically have COPs around 0.5 (Herold, Radermacher & Klein, 1996). As a refrigerant, ammonia (NH_3) is superior to water in the low refrigeration temperatures achievable by its use. While water's freezing temperature is 0°C at standard conditions, ammonia's is -77.7°C, which allows an ammonia-water absorption chiller to achieve refrigeration temperatures much lower than a water-lithium bromide chiller. In fact, subzero refrigeration is the greatest advantage of an ammonia-water absorption chiller, making this technology useful for ice production, food processing, cold storages, and other applications requiring a subzero chilling demand. One drawback of ammonia is that, with a boiling point of -33.35°C, its vapor pressure is exceedingly high. For this reason, the generators of ammonia-water chillers require very high pressures for temperatures typically encountered in that component. While ammonia's high vapor pressure permits a reduction in pipe diameter and in the size of heat exchangers in an ammonia-water absorption chiller, the work of the solution pump in an ammonia-water chiller must increase and is no longer negligible, as in a water-lithium bromide chiller. Additionally, ammonia is toxic, so the use of ammonia-water chillers is usually restricted to well-ventilated areas, although small residential units are frequently used inside without any toxicity issues arising. Ammonia-water absorption chiller hardware will be discussed in more detail later in this chapter.

2.3 Mixture Properties

One challenge that the study of absorption chiller systems poses is understanding the thermodynamics of mixtures, which behave very differently from a pure substance, like the working fluid in a conventional vapor compression chiller. Understanding the properties of a mixture of water-lithium bromide or ammonia-water is essential in calculating the conditions at the state points in the chiller's solution loop, as will be done in the Engineering Equation Solver study presented in the next chapter. The properties of ammonia are widely available and well-documented; however, the same is not true of lithium bromide. Appendix B includes a list of papers that explore the properties of water-lithium bromide solutions, as well as an enthalpy-mass fraction diagram for water-lithium bromide.

2.3.1 Mixture's Temperature-Concentration Diagram

One means of understanding the thermodynamics of a mixture is graphically through the use of a temperature-mass fraction, or temperature-concentration, diagram (T-x diagram). Here, the mass fraction is defined as the ratio of the mass of one component to the mass of both components. Figure 2.2 is an example of an evaporation process of a mixture of two generalized substances represented qualitatively on a T-x diagram, where *x* is the mass fraction of component B. In a water-lithium bromide absorption chiller, a T-x diagram can be used to represent the evaporation of refrigerant water out of a solution of water-lithium bromide in the chiller's generator. Compared to Figure 2.2, the T-x diagram for a mixture of water and lithium bromide would have a much steeper ellipsoidal region between the boiling line and dew line because lithium bromide's boiling temperature (1265°C, or 1538K) is slightly more than four times that of water (100°C, or 373K).

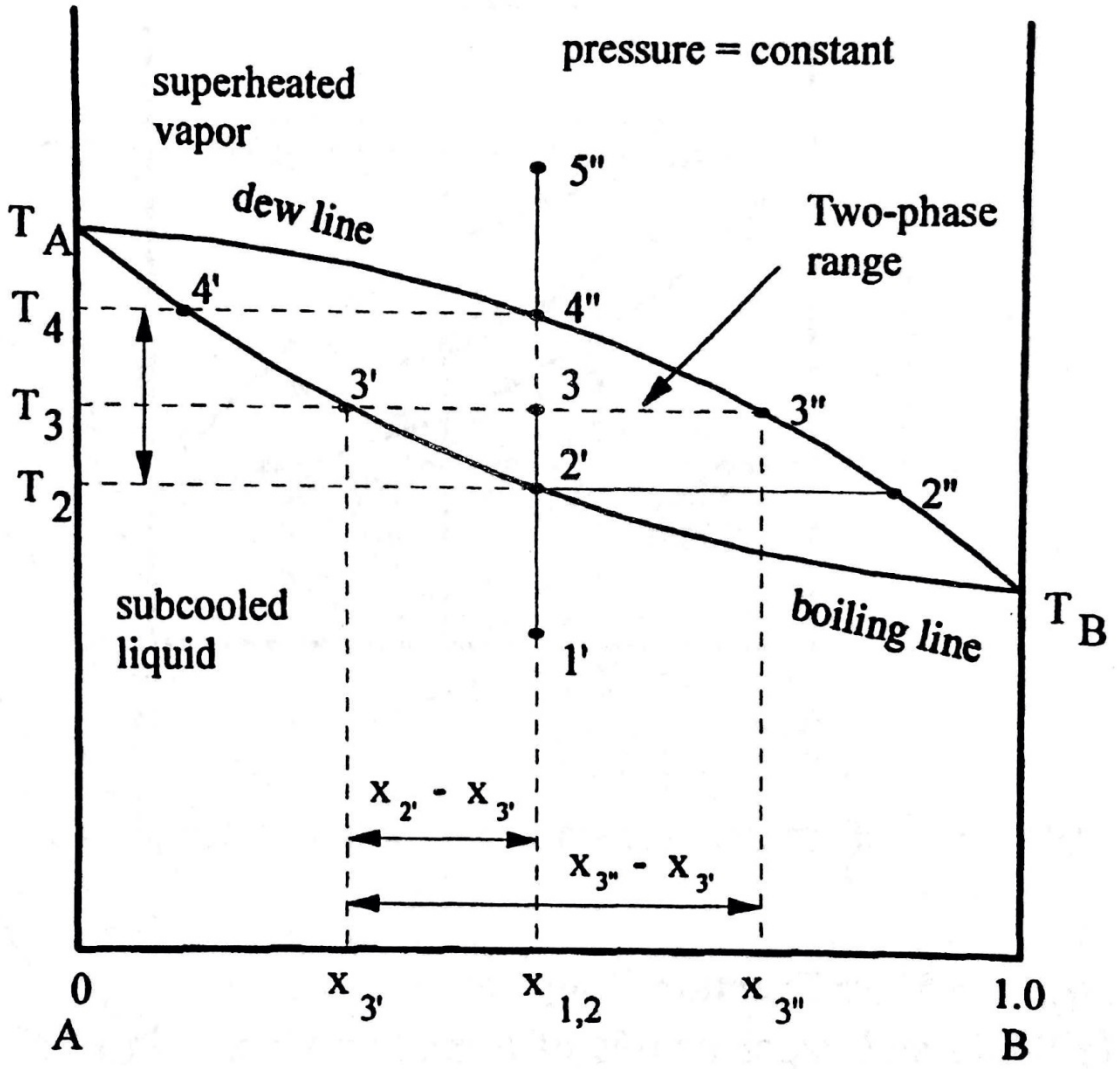

Figure 2.2 Qualitative evaporation process of a two-substance mixture on a T-x diagram (Herold, Radermacher & Klein, 1996)

In Figure 2.2, two substances are present in solution—substance A and substance B. A point with a single prime indicates the liquid phase, and a double prime indicates the vapor phase. The boiling point of substance A is T_A, and the boiling point of substance B is T_B, which is lower than the boiling point of substance A. This also means that the vapor pressure of substance B is higher than the vapor pressure of substance A at the specified pressure.

The evaporation process in Figure 2.2 begins with a solution of roughly 50% mass fraction of substance A and 50% mass fraction of substance B in the subcooled liquid phase at

state 1’. As the solution is heated, it reaches the boiling line at state 2’; and the first vapor bubbles of substance B form. State 2” represents the vapor mass fraction of substance B that is in thermal equilibrium with the liquid of state 2’. Moving from state 2' to state 2" implies that more of substance B evaporates into vapor as the mass fraction of B increases in the mixture at a constant temperature. As heat is further added to the solution, the mass fraction of substance B in the liquid phase and the mass fraction of substance B in the vapor phase (in thermal equilibrium with its liquid phase) decrease to states 3’ and 3”, respectively. This implies that liquid substance B starts to evaporate at lower mass fraction (or lower B-concentration in the mixture) as temperature increases. At 3”, there is more of substance A in the vapor phase than there is at state 2”. The vapor quality of the mixture at state 3 can be found by taking the ratio of $x_{2'}$-$x_{3'}$ to $x_{3''}$-$x_{3'}$, as shown in the figure. Next, additional heat is added to the mixture and complete evaporation of substance B is achieved at state 4”, where the vapor mass fraction of substance B equals its original liquid mass fraction at state 1’. That is, all of substance B’s original liquid content is now in the vapor phase. Adding additional heat to the mixture produces a superheated vapor at state 5”.

2.4 The Inner Workings of a Single-Effect Absorption Chiller

In Chapter 1, a basic description of the single-effect absorption chiller cycle is presented using a block flow diagram. Figure 2.3 gives a more detailed view of the internals of such an absorption chiller. A single-effect absorption chiller is a two-pressure device. Housed in the lower shell, the absorber and evaporator are at the system’s low pressure; housed in the upper shell, the condenser and generator are at the system’s high pressure. The cycle proceeds in the following way. Dilute, or weak, water-lithium bromide solution in the absorber at state 1 is pumped from the system’s low pressure by the solution pump, which increases the pressure of the weak solution to the system’s high pressure at state 2. The dilute solution passes from the pump outlet through the tubes of a shell and tube heat exchanger (immediately on the left of the pump) where it is preheated by the strong solution leaving the generator.

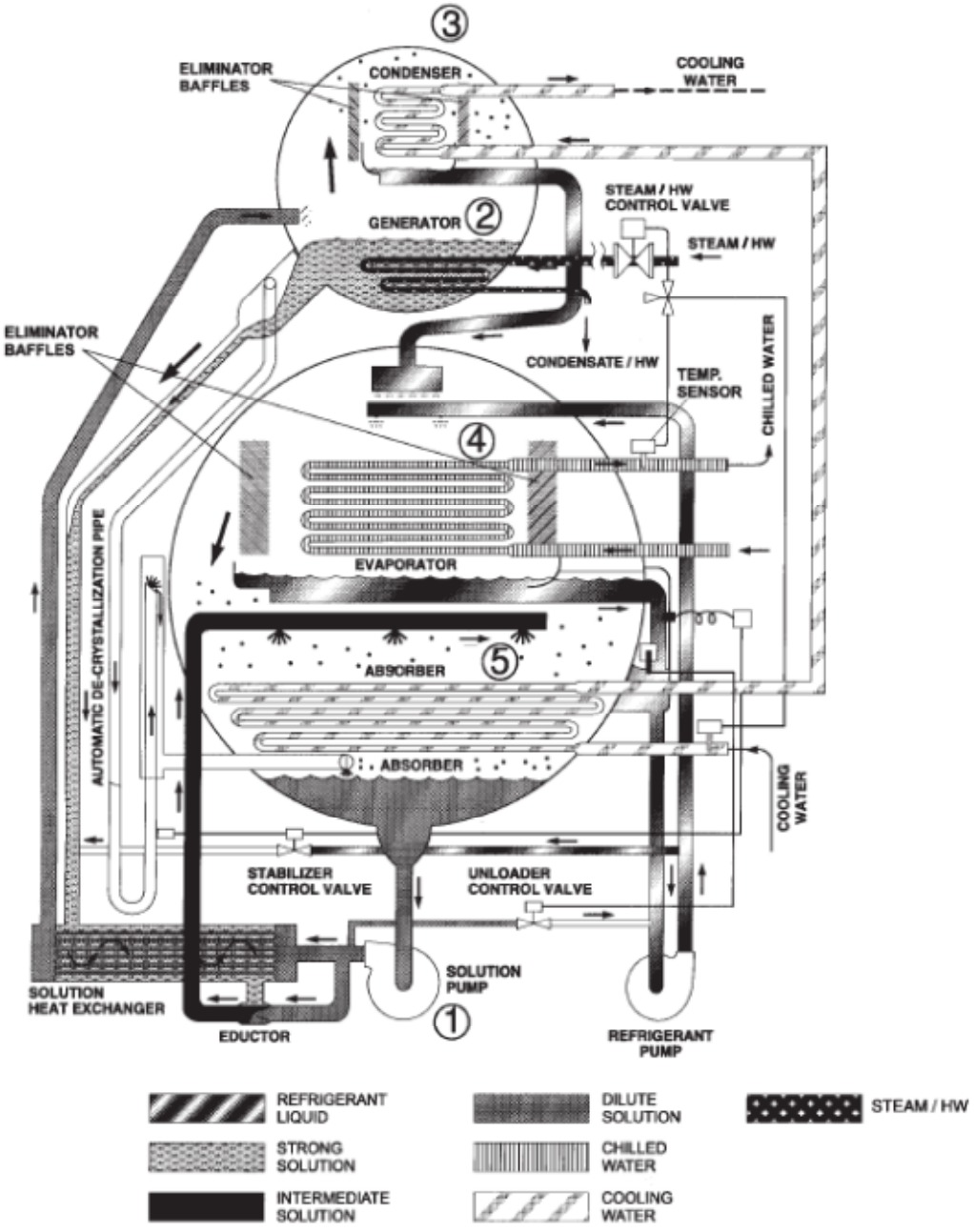

Figure 2.3 Hot water-/steam-driven single-effect lithium bromide absorption chiller internals (Source: Johnson Controls, Inc., 2010)

The dilute solution then flows to the chiller's generator (state 2) where it is heated by the heat input that drives the cycle. In the chiller in Figure 2.3, the driving heat input is steam or hot water that passes through coiled tubes that are immersed in the solution in the generator. Heat is transferred from the hot water / steam in the tubes to the dilute solution in the

generator, and a portion of the refrigerant water in the dilute solution evaporates out of the solution, leaving a solution more concentrated in lithium bromide absorbent, or strong solution, in the generator. This strong solution flows back to the absorber by gravity. During its path back to the absorber, it goes through an exchanger to preheat the weak solution coming out of the solution pump state earlier. The refrigerant water vapor travels upward to the condenser heat exchanger where it condenses to a saturated liquid, which pools below the condenser tubes and is gravity fed through a throttling process by being sprayed over the evaporator heat exchanger tube bundle at state 4. Due to the significant pressure reduction through the throttling process of the spraying head, the refrigerant flashes into vapor and absorbs latent heat in the evaporator. The spraying process adds heat transfer effectiveness by breaking down the liquid refrigerant into small droplets. The refrigerant droplets flash and absorb heat from the ambient water circulating through the tubes. The unevaporated liquid refrigerant is recycled back to the evaporator through a refrigerant pump and is sprayed again in the evaporator. The absorption of heat from the circulating ambient water by the refrigerant in the evaporator provides the absorption chiller's cooling effect. That is, the ambient water stream exits the evaporator heat exchanger's tube bundle at a lower, more chilled, temperature.

A single-effect lithium bromide absorption chiller operates at near vacuum pressures. The system's pressure in the lower shell may be as low as 0.600 kPa. At this pressure, water boils at approximately 1°C. Therefore, the heat content of the ambient water (typically 7°C) passing through the evaporator heat exchanger's tube bundle is sufficient to evaporate the refrigerant liquid after throttling. The refrigerant water exits the evaporator as a saturated vapor and enters the bottom part of the lower shell where it mixes exothermically with strong absorbent solution in the absorber. Cooling water circulates through the absorber heat exchanger tube bundle and cools the absorber to promote complete dissolution of the water vapor into the strong solution, yielding dilute solution. This dilute solution is pumped by the solution pump through the solution heat exchanger, and the cycle repeats itself. The COP of single-effect absorption chillers, like the one in Figure 2.3, is typically around 0.7.

2.5 Double-Effect Water-Lithium Bromide Absorption Chiller

Figure 2.4 shows a double-effect water-lithium bromide absorption chiller cycle. A double-effect chiller cycle can be compared to that of a two cascading single-effect chillers. There are, however, a few major differences between a single-effect and double-effect absorption chiller. A double-effect absorption chiller contains two condensers—a low-pressure condenser and a high-pressure condenser; two generators—low-pressure and high-pressure; two solution pumps; and two solution heat exchangers.

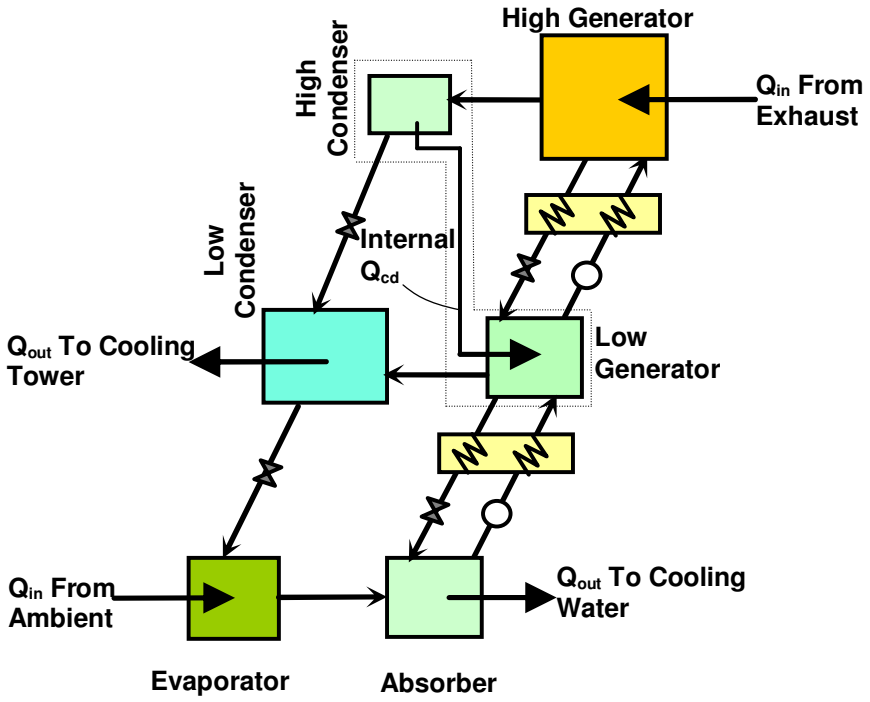

Figure 2.4 Double-effect water-lithium bromide absorption chiller

Another major difference between the single-effect and double-effect configurations is that, unlike a single-effect absorption chiller, a double-effect chiller is a three-pressure device. The high generator, which receives the thermal input that drives the cycle, and the high condenser are at the system's high pressure. The low generator and low condenser are at the system's intermediate pressure, and the evaporator and absorber are at the system's low pressure. Other than the additional components and the addition of an intermediate system pressure, the other major difference between a single-effect and double-effect absorption

chiller is that, rather than rejecting heat to a cooling tower, as the low condenser does, the high condenser transfers its heat internally to the low generator. This heat input to the low generator from the high condenser drives the bottom half of the absorption cycle. The modifier *double-effect* comes from the fact that the driving heat input to the high generator is utilized two times in the chiller—once to generate vapor in the high generator and again to generate vapor in the low generator by the internal heat transfer from the high condenser just described. The major advantage of the double-effect configuration is that the high generator can accept a higher temperature heat input than a single-effect configuration and is, therefore, able to better utilize the heat input available to it to further increase its chilling capacity beyond that of a single-effect chiller. The COP of a double-effect lithium bromide chiller ranges from 1.1-1.3, which is higher than the COP of the single-effect configuration; but this increase comes with a higher capital cost and an increase in the size and weight of the chiller.

2.6 Single-Effect Ammonia-Water Absorption Chillers

Some properties of using ammonia-water as the working fluid pair are discussed earlier in this chapter. The ammonia-water absorption chiller cycle operates according to the same working principles as in a single-effect water-lithium bromide, but some issues arise in ammonia-water chillers due to the unique properties of this working fluid pair.

The major issue encountered in ammonia/water chillers results from using water as the absorbent. Water is volatile and has a vapor pressure that is close to ammonia's. When ammonia is vaporized from the strong solution in the generator, it carries with it small amounts of water. Herold and Radermacher detail an ammonia/water chiller's performance decline resulting from the volatility of water (1996). The ammonia vapor and water pass through the condenser and into the evaporator, where the water tends to accumulate, subsequently causing a pressure drop in the evaporator. This pressure drop causes a shift in the chiller's design point, which necessitates lowering the absorber's cooling water temperature for the ammonia vapor still to be able to be absorbed by the absorbent water. Consequently, the temperature in the generator must increase. The overall effect of water accumulation in the evaporator is to lower the COP of the ammonia/water absorption chiller. Two commonly

employed options for increasing the overall performance of an ammonia/water chiller are a rectifier and a condensate precooler.

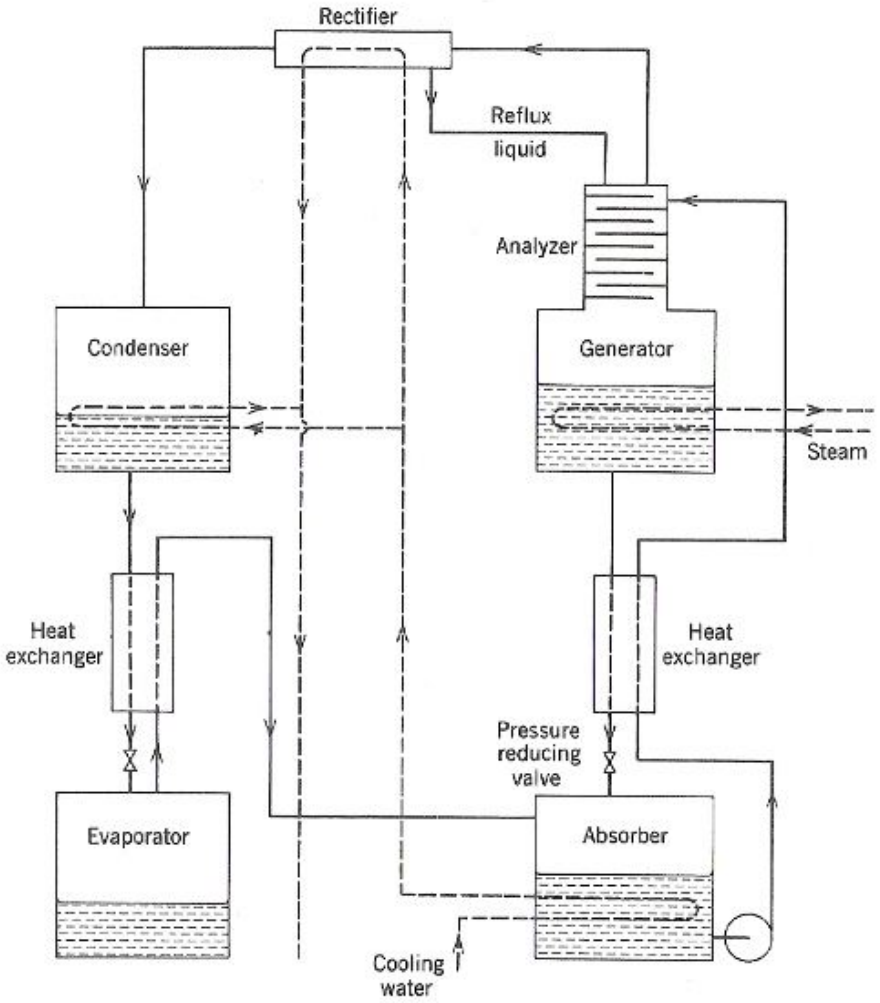

Fig. 20-22 Ammonia-water absorption system.

Figure 2.5 Single-effect ammonia-water absorption chiller with rectifier and condensate precooler heat exchanger (Source: Khemani, 2010)

A rectifier, as depicted in Figure 2.5, is an internal heat exchanger that uses the weak ammonia-water solution, after it passes through the solution pump, to cool the refrigerant vapor leaving the generator. Cooling the ammonia vapor after the generator causes the water in the vapor to condense, removing the water from the vapor stream flowing to the condenser so that it will not subsequently accumulate in the evaporator. The condensed water in the

rectifier is returned to the generator, and the weak solution flows from the rectifier through the solution heat exchanger where it is preheated before entering the generator. Nonetheless, trace amounts of water could still remain in the ammonia vapor after rectification. However, because the mass fraction of the water in the vapor is reduced in the rectifier, the amount of water that collects in the evaporator decreases. The result is an improvement in the chiller's performance.

Another option for improving the performance of an ammonia/water absorption chiller is to use a condensate precooler. Condensate precooling is an internal heat exchange process that uses the ammonia vapor leaving the evaporator to subcool the ammonia condensate from the condenser, thus lowering the enthalpy of the refrigerant at the evaporator inlet. Because the enthalpy of the refrigerant at the evaporator exit stays the same, the cooling capacity of the evaporator increases. Moreover, any water that accumulates in the evaporator can be evaporated in the condensate precooler. Though condensate precooling causes a pressure drop in the evaporator, this drop in pressure is not as deleterious as without precooling; and the performance of the chiller usually increases. Still, even with rectification and condensate precooling, the COP of a typical single-effect ammonia/water absorption chiller is about 0.5.

2.7 Summary: Water-Lithium Bromide & Ammonia-Water Absorption Chillers

With fewer components and higher performance, water-lithium bromide absorption chillers tend to be a better choice in applications not requiring subzero refrigeration temperatures. Unlike ammonia, lithium bromide is non-toxic. Also, lithium bromide has a much lower vapor pressure than water. For this reason, water can evaporate from the strong solution in the generator without carrying trace amounts of lithium bromide salt with it. This allows lithium bromide chillers to eliminate the additional components, like a rectifier and condensate precooler, that ammonia-water chillers implement. Water-lithium bromide absorption chillers have higher coefficients of performance than ammonia-water chillers. Overall, water-lithium bromide chillers are more widely used than ammonia-water chillers or chillers using a non-conventional working fluid because they are more efficient and more reliable than other absorption chillers and because LiBr salt is non-toxic, a major advantage in residential

applications. In the end, among other factors, selection of a working fluid depends on the required refrigeration temperatures of the intended application and the need for high performance.

Table 2.1 Comparison of water-lithium bromide and ammonia-water absorption technology

Parameter	Water-Lithium Bromide	Ammonia-Water
Relative Capital Cost	**Low**	**High**
Available Sizes (RT)	**5-1660**	**2-1000**
Single-Effect COP	**0.7**	**0.5**
Lowest Refrigeration Temperatures (°C)	**0**	**-77.7**
Relative Volatility of Refrigerant to Absorbent	**Good**	**Poor**
Refrigerant Latent Heat (kJ/kg)	**2260**	**1369**
Toxicity	**Non-toxic**	**Toxic**

CHAPTER THREE

DISCUSSION OF VARIOUS DESIGNED CASES

Existing micro-CCHP systems typically consist of a reciprocating engine or microturbine prime mover, a heat recovery unit, a thermally activated device, and a cooling tower. The thermal efficiency of existing systems, pre-packaged or otherwise, ranges from 60-90%. While existing systems offer significant fuel savings and higher efficiencies than systems that do not utilize a cogeneration configuration, such systems can be made more efficient and achieve higher system performance through certain design modifications. This chapter will discuss details of the existing micro-CCHP systems using 100 kW (HHV) of microturbine fuel input as a basis selected for the convenience of easily comparing the different system configurations discussed. Then, different options of increasing the efficiency of existing systems, such as gas turbine inlet cooling, will be explored. Later, the systems explored in this chapter are scaled up to the actual fuel input using the specs of an available Capstone microturbine. Finally, the details and results of an Engineering Equation Solver calculation routine that was developed to examine the states in an absorption chiller will be discussed herein in an effort to examine the characteristics of the absorption chiller to ensure the designed parameters are within exisiting industrial norms.

3.1 Existing Micro-CCHP Systems

A conventional micro-CCHP system with a microturbine, heat recovery unit, absorption chiller, and cooling tower is depicted in Figure 3.1. The absorption chiller in this configuration is a 9.7RT (Refrigeration Ton) single-effect system with a Coefficient of Performance (COP) of 0.7206, and the prime mover is a 30 kW Capstone C30 microturbine. At ISO conditions (60% relative humidity (RH) and 15^{o}C (59^{o}F)), for every 100 kW (HHV) fuel input (low pressure natural gas), the system can produce 22.9 kW of electricity, 34.2 kW chilled water, and 12 kW hot water. The energy budget in Figure 3.2 shows the useful products of the conventional micro-CCHP system. *A fuel input of 100 kW is used for convenience. The actual rated fuel input is 122.2*

kW (HHV) or 111.11 kW (LHV), according to the manufacturer's specifications (Capstone Turbine Corporation, 2002); and the actual rated power output is 28 kW.

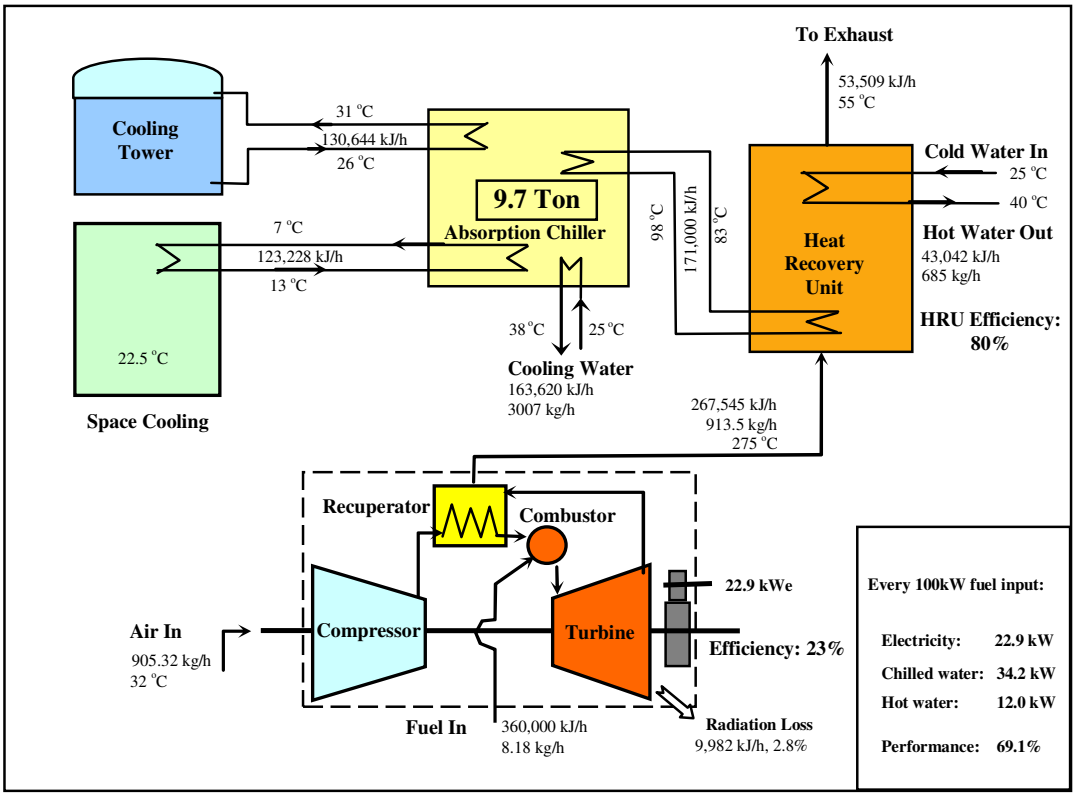

Figure 3.1 Conventional micro-CCHP system with MGT, HRU, standalone ACS, and cooling tower

For this conventional micro-CCHP system, the overall thermal/electric efficiency is approximately 69.1% (HHV). This efficiency is on the high end of the performance range of existing small-size systems, which have thermal efficiencies ranging from 60-70%. In comparison, the efficiency of large-size systems typically ranges from 80-90%.

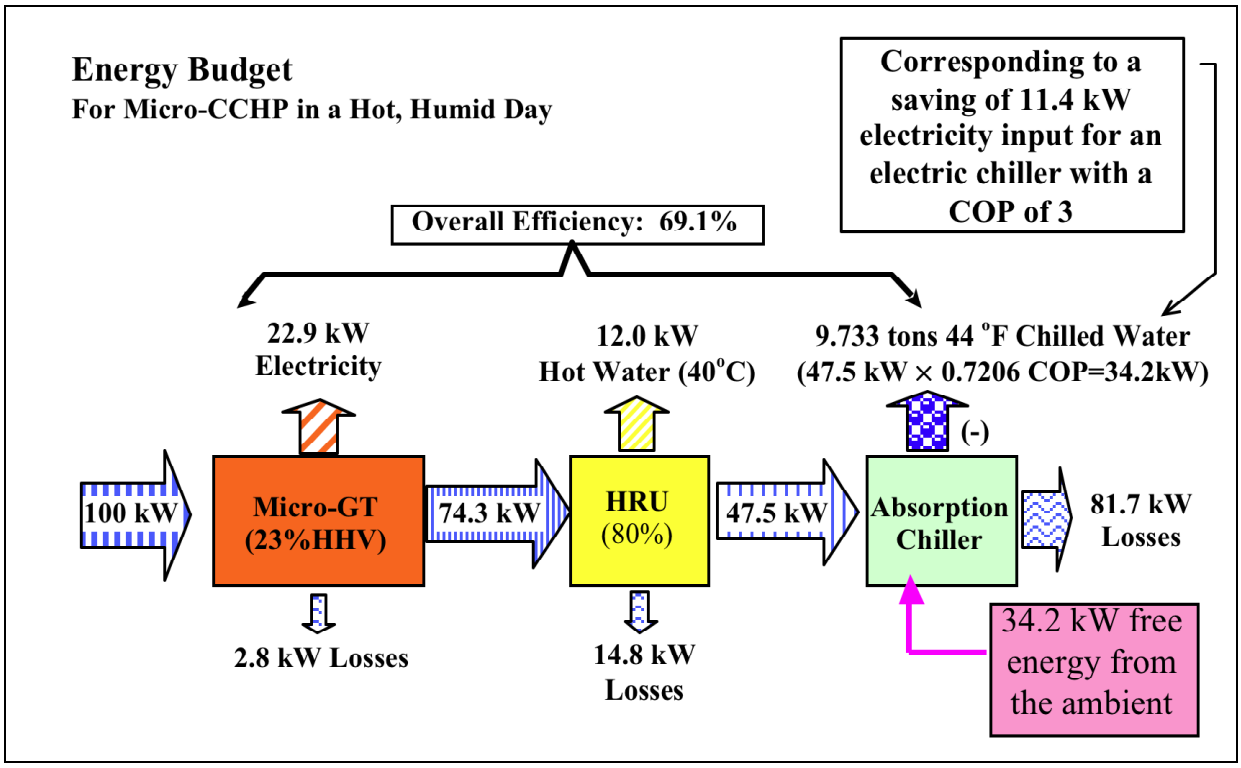

Figure 3.2 Energy budget for conventional micro-CCHP system in Fig. 3.1

3.1.1 Explanation of Energy Budget

The energy budget (Fig. 3.2) accounts for 2.8 kW of radiation losses in the microturbine. The electricity output and efficiency of the microturbine are determined from Figure 3.3, which shows that an increase in ambient temperature causes the efficiency of the turbine to decrease. On a hot, humid day, the ambient temperature may be close to 95°F, which corresponds to a turbine net thermal efficiency of approximately 22.9%. For 100 kW of fuel input at the stated ambient conditions, the microturbine will output 22.9 kW electrical power. The total microturbine exhaust energy, according to the manufacturer's specifications, will be 74.3 kW. The turbine exhaust enters the heat recovery unit (HRU). A liberal value of 80% is taken for the heat recovery unit efficiency; therefore, the associated HRU losses amount to 14.8 kW per 100 kW of microturbine fuel input. Depending on the hot water needs of the application, the amount of hot water produced can be varied. For this particular design, 12.0 kW of hot water is desired, leaving 47.5 kW as the driving heat input to the generator in the absorption chiller.

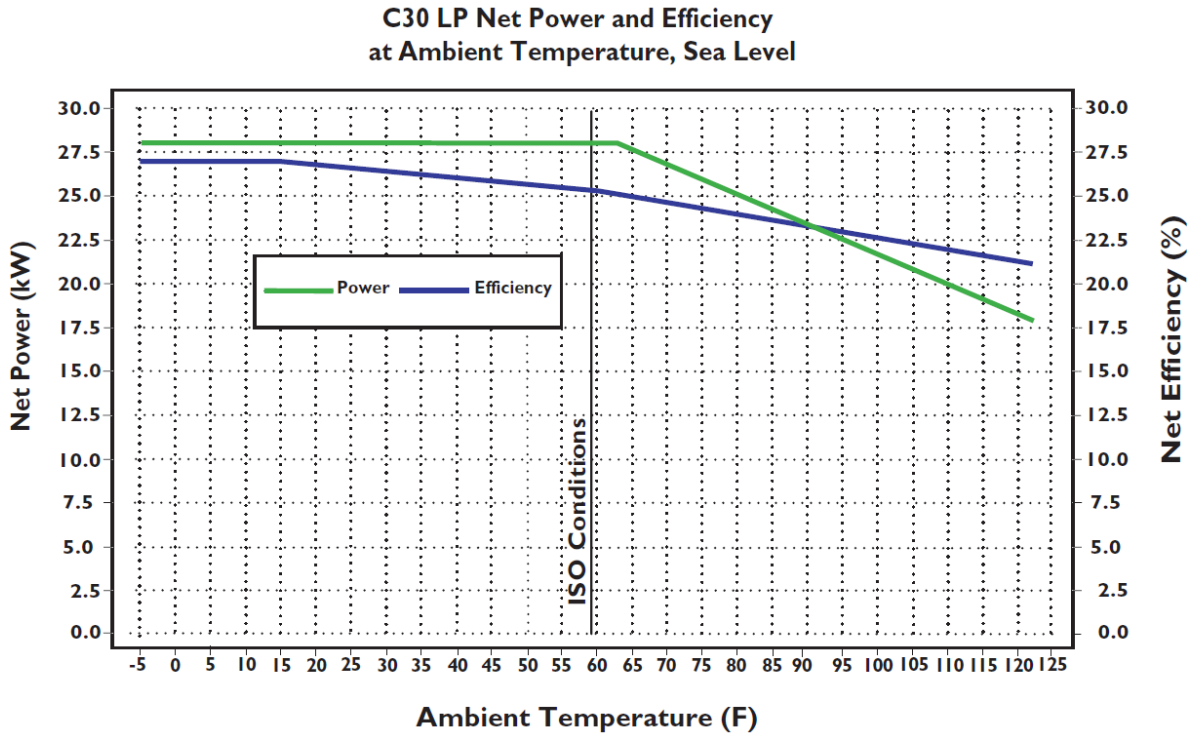

Figure 3.3 De-rating of Capstone C30 microturbine efficiency (LHV) and power output due to ambient temperature (Source: Capstone Turbine Corporation, 2002)

Using typical single-effect absorption chiller design conditions (ASHRAE Handbook 2001 Fundamentals) for the mass flow rate and temperature difference of the water in the evaporator's external heat exchanger loop, the heat absorbed by the evaporator is calculated to be 34.2 kW. The COP of the absorption chiller is, therefore, 0.72. Since the 34.2 kW of energy absorbed by the evaporator comes from an ambient air/water stream, it is counted as "free energy" in the energy budget; it is a designed useful product, as it provides space-cooling or refrigeration corresponding to the desired need. Should an equivalent amount of chilled water be produced by an electric chiller with a COP of 3, the required electrical input would be 11.4 kW. While an electric chiller has a higher COP than a single-effect LiBr-H_2O absorption chiller and requires less energy to produce the same cooling capacity, in a CCHP system, the energy for chilling comes from the MGT's waste heat and is thus provided at no additional fuel cost to the user. Finally, the energy losses (81.7 kW) in the absorption chiller are the heat rejected to the cooling tower (36.3 kW) and the heat rejected to the absorber cooling water stream (45.4 kW), which will be explained in more detail later.

3.1.2 Disadvantages of Existing Systems

There are several disadvantages of the existing system in Figure 3.1:

- The energy rejected by the cooling tower is wasted.
- A separate absorption chiller, heat recovery unit, and cooling tower limit the overall efficiency of the system, occupy a lot of space, are more cumbersome to install, and increase capital cost.
- The efficiency of the microturbine is low, and its output suffers from hot summer temperatures (Fig. 3.3).
- The high energy microturbine exhaust cannot be effectively utilized via a separate ACS and HRU.

3.2 Proposed Micro-CCHP System Improvements

To eliminate the disadvantages of the existing system, the following measures are proposed. First, a portion of the chilled water can be used to cool the inlet air of the microturbine to increase its efficiency to that of ISO conditions when ambient temperatures are high. Second, the heat rejected from the absorber and the condenser to the environment can be recovered by being redirected to heating the hot water to the user. By doing this, the cooling tower is eliminated from the system configuration and, with it, its required space and capital cost. Third, the heat recovery unit can be integrated into the generator of the absorption chiller. This removes an entire component from the existing system, which reduces the size and capital cost of the system. Additionally, integrating the HRU into the generator of the ACS will improve its heat recovery efficiency.

3.2.1 Gas Turbine Inlet Cooling

Because combustion turbines are constant volume machines, denser air provides for greater mass flow. The hotter the turbine inlet air, the less dense that air is. Therefore, cooling the inlet air decreases the air's density and increases the air mass flow into the turbine. Mohanty and Paloso (1995) show that reducing the temperature of gas turbine compressor

intake air from ambient condition to ISO condition can increase the turbine's power output by 8 to 13%. Mohanty and Paloso were able to achieve gas turbine inlet cooling by using a double-effect lithium bromide-water absorption chiller in a hot, humid climate.

Wang and Braquet (2008) shows that gas turbine inlet cooling is highly effective in counteracting the decrease in gas turbine performance due to elevated ambient temperatures. The results of Wang's research show that gas turbine output is a strong function of ambient temperature, typically losing between 0.3% and 0.5% of its ISO rated power for every 1°F rise in inlet temperature.

Figure 3.3 shows the benefit of inlet cooling. On an 85°F day, inlet cooling to ISO condition (59°F and 60% relative humidity) will enhance electric output by 15%. On a 95°F day, the electric power output can be enhanced by 20% by implementing inlet cooling. To further increase microturbine electric output, the inlet air can be cooled even further to 42°F, which would provide for a 10% increase in output.

There are many methods of cooling turbine inlet air, including indirect evaporative "pre-cooling" systems, active "chiller" refrigeration based systems that are either electrically driven or thermally driven, dessicant cooling systems, and a variety of water spray or fogging options. This study proposes that a portion of the absorption chiller's cooling capacity be used to provide the gas turbine inlet air cooling for the Capstone C30 microturbine by placing the chiller's evaporator in front of the compressor inlet of the turbine. By doing this, it is understood that the refrigeration or spacing cooling capacity will be reduced accordingly.

3.2.2 Integrating the Cooling Tower Function into the Absorption Chiller

A cooling tower functions as a heat sink for the condenser of an absorption chiller. In a typical cooling tower employed in a micro-CCHP system, water that is at a lower temperature than the refrigerant vapor exiting the generator circulates in a closed loop and cools the condenser. In the integrated chiller in Figure 3.4, a single stream of city water, which is usually supplied at a temperature below 80°F (27°C), will provide cooling for both the absorber and the condenser. This cooling water stream will absorb the heat released by the exothermic

reaction—the absorption of refrigerant (water vapor in this study) by lithium bromide solution—in the absorber. The cooling water continues to flow from the exit of the absorber at state point 14 to the inlet of the condenser. It passes through the condenser where it absorbs the latent heat released by the condensing of the refrigerant vapor and exits the condenser at state point 16. At this point, the cooling water has absorbed the heat rejected in the absorber and the condenser and is now warm. The water is further heated in the generator by a portion of the microturbine exhaust gas. The following section details how this is achieved. By routing the cooling water in this way, the standalone cooling tower is eliminated. The energy typically rejected to the cooling tower is now utilized in the new system design, instead of being wasted as it is in conventional systems. Moreover, the capital cost and space required for the cooling tower are eliminated from the new system.

3.2.3 Heat Recovery Unit Integration

The generator functions as a liquid-vapor separator, separating refrigerant vapor from the absorbent solution by the addition of the driving heat from the energy source—in this case, from the microturbine exhaust. The generator typically occupies a large volume of the absorption chiller. Integrating the heat recovery unit into the integrated chiller design requires the addition of a compact heat exchanger inside the generator. This will allow the temperature of the water to be raised according to the needs of the application by passing it through the generator in a separate path to be heated by the microturbine exhaust gas. Figure 3.4 shows the heat recovery unit integrated into the generator. In this figure, the net heat input between state points 11 and 12 is dedicated to driving the absorption chiller cycle, while the net heat input between state points 12 and 20 is dedicated to heating the water stream that flows through the absorber, condenser, and generator components, and is output as useful hot water at state point 19. By redesigning the generator heat exchanger, the standalone heat recovery unit is eliminated, and the space, cost, and system irreversibility of such a standalone unit is significantly reduced.

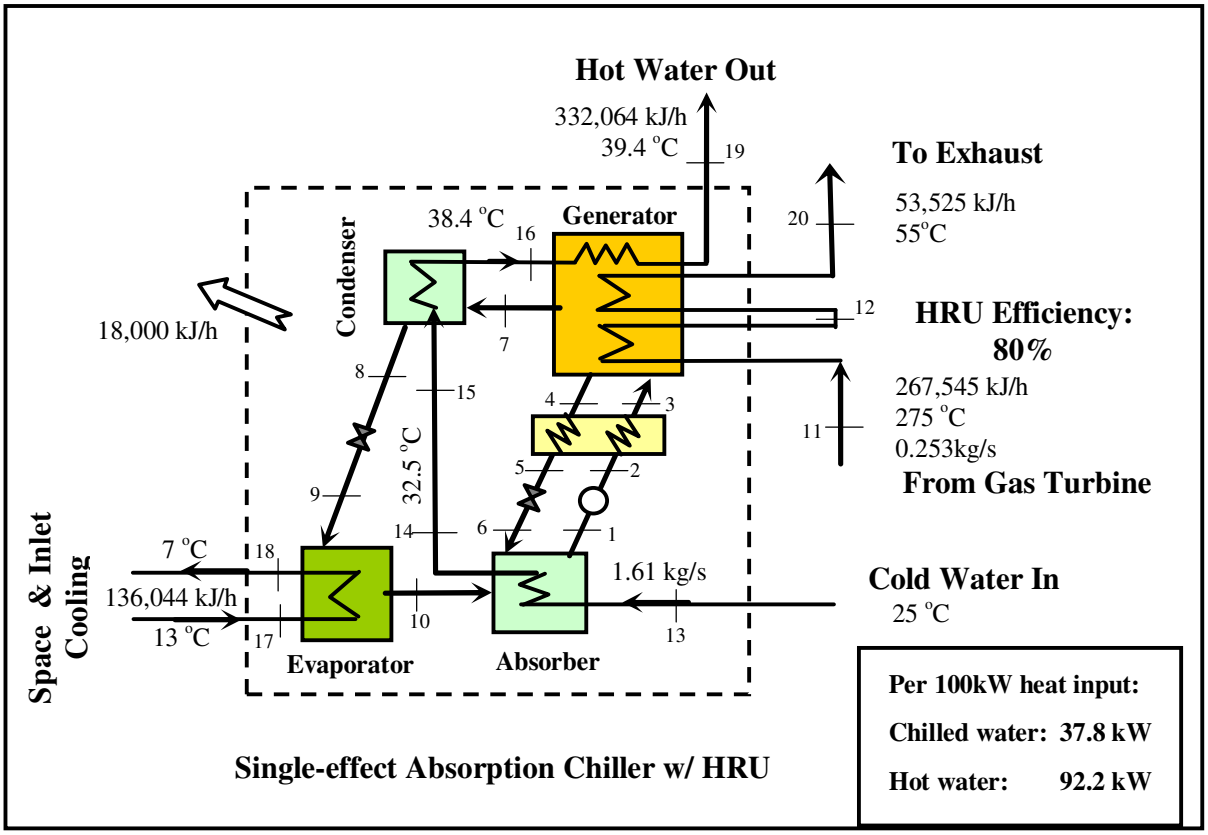

Figure 3.4 Integrated single-effect absorption chiller with HRU in generator and condenser heat rejection redirected to the generator HRU

3.3 Micro-CCHP System Design Concept 1 with Integrated Single-Effect Absorption Chiller

Figure 3.5 provides a schematic of the conceptual design of the proposed micro-CCHP system that employs the integrated single-effect absorption chiller from Figure 3.4 above. The proposed improvements to existing conventional systems—gas turbine inlet air cooling, integration of the heat recovery unit into the absorption chiller's generator, and elimination of the cooling tower—are implemented in this system. The energy budget for the improved system design is provided in Figure 3.6.

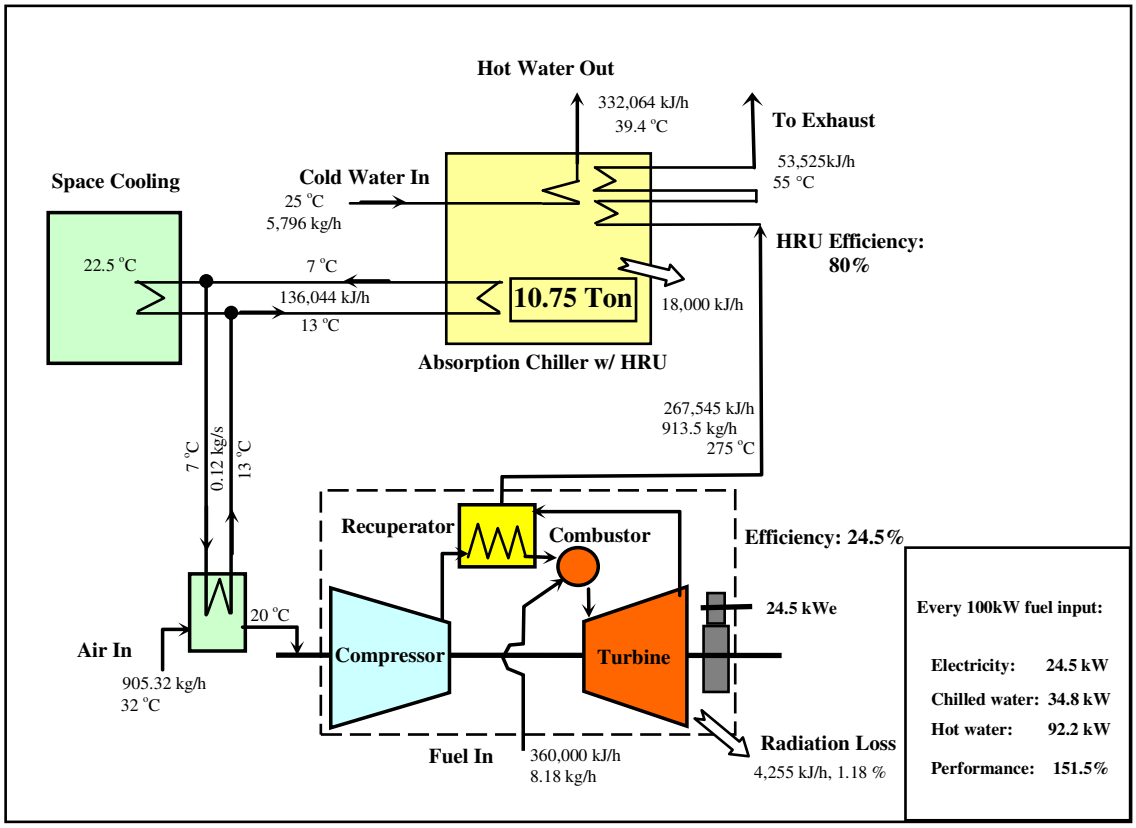

Figure 3.5 Micro-CCHP design concept 1 with integrated HRU, microturbine inlet cooling, and cooling tower removed

There are several noticeable differences between the energy budget for the existing conventional system in Figure 3.5 and the budget for design concept 1. First, more heat (52.45 kW) enters the generator of the single-effect chiller with the integrated HRU than it does in the standalone single-effect chiller in Figure 3.1. This increase in the driving heat input results in an associated increase in the evaporator cooling capacity. The energy increase in both components is proportional; therefore, the COP of the integrated single-effect absorption chiller is still 0.7206, as it is for the standalone chiller in the existing system. However, a rise in the evaporator's cooling capacity improves the potential for gas turbine inlet cooling. Here, cooling the microturbine inlet air with 3.0 kW of chilled water bled from the evaporator provides an electricity enhancement of 1.6 kW for every 100 kW (HHV) of fuel input. Second, the new design allows for 92.2 kW of hot water to be produced, compared to 12.0 kW in the existing system. The reason for this drastic increase in hot water production, as shown on the energy budget, is the pre-heating of the water using the heat captured from the absorber and the

condenser, as discussed in Section 3.2.2. Utilizing the heat captured from the absorber and the condenser to augment the useful hot water energy product also accounts for the decrease in absorption chiller losses here, whereas that energy is wasted and is considered as losses in the existing system. This system produces an equivalent savings of 11.6 kW of electricity, which would be required to produce 9.9 RT of chilled water at the peak load rate based on an electric chiller with a COP of 3.

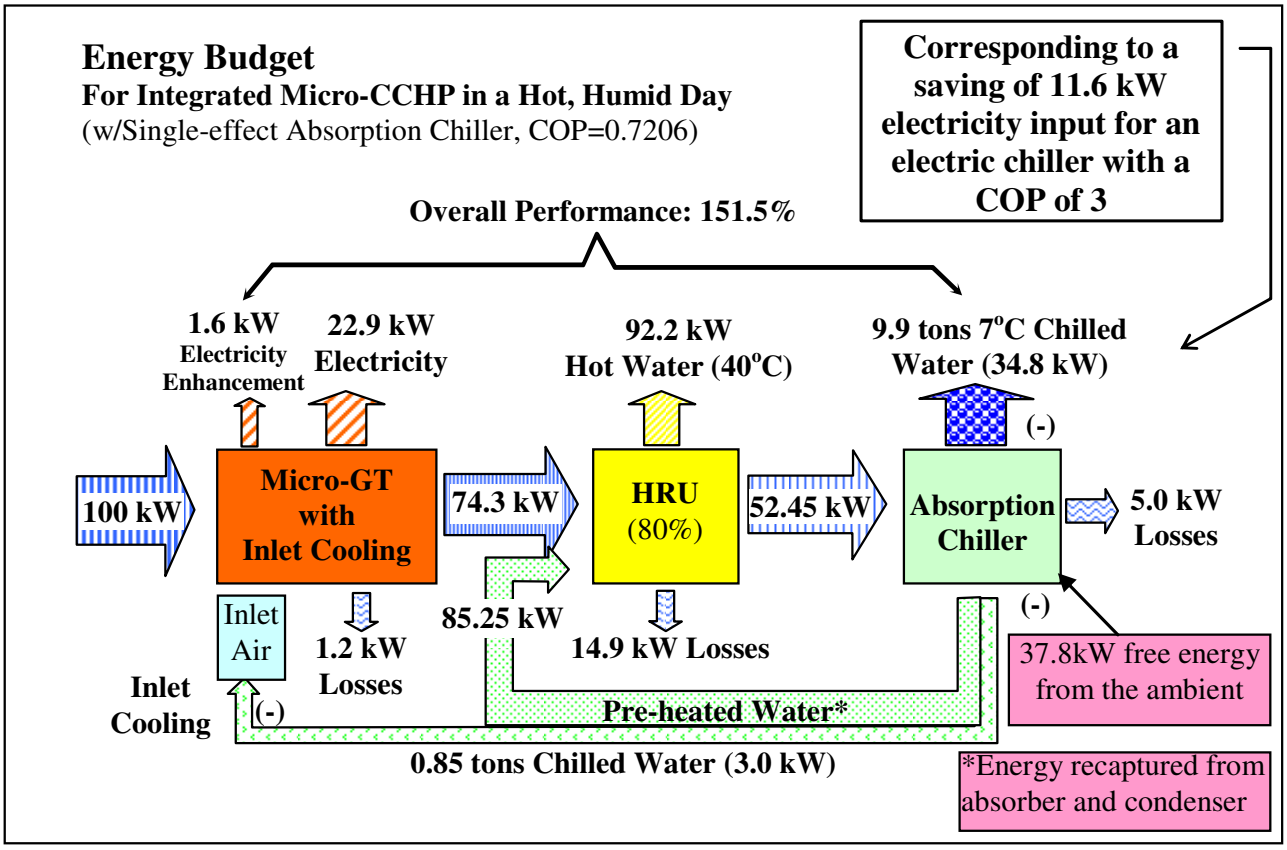

Figure 3.6 Energy budget for micro-CCHP concept design 1—integrated single-effect chiller and 100 kW (HHV) fuel input

The total savings includes 1.6 kW of electricity enhancement, 11.6 kW electricity savings to produce an equivalent amount of cooling, and the fuel cost to produce 92.2 kW of hot water at 40°C (104°F.) The overall performance of micro-CCHP system of design concept 1—commonly defined in polygeneration applications as the energy content of the system's useful products divided by the energy of the prime mover's fuel input—is 151.5%, whereas it was 69.1% for the existing system. It is important to note that 151.5% is a performance value and

not an efficiency, which cannot exceed 100%. The part of the energy beyond 100% is harvested from the environment by way of the absorption chiller. The 3 kW of chilled water used to cool the microturbine inlet is not counted in the overall performance because the resulting 1.6 kW enhancement in microturbine electric output has already been counted.

3.4 Micro-CCHP System Design Concept 2 with Integrated Double-Effect Absorption Chiller

Because the microturbine's exhaust gas is at a relatively high temperature of 275°C—higher than that of a reciprocating engine—the second design concept seeks to better utilize the high temperature exhaust by employing a double-effect absorption chiller, which typically has a COP of 1.3. A higher COP for a fixed driving heat input equates to an increase in cooling capacity. Figure 3.7 shows the integrated double-effect absorption chiller used in design concept 2. As with the integrated single-effect chiller, the integrated double-effect chiller integrates the heat recovery unit into the generator. In a double-effect absorption chiller, which has two generators, the exhaust heat is input to the high generator; therefore, the heat recovery unit is integrated into the high generator. In the double-effect schematic, the net heat input between state points 21 and 22 in the high generator is dedicated to driving the double-effect cycle, while the net heat input between state points 22 and 30 is dedicated to heating the water stream that flows through the absorber, low condenser, and high generator components, and is output as useful hot water at state point 31. Also similar to the integrated single-effect chiller is the redirection of the condenser heat rejection to the generator HRU. In a conventional double-effect absorption chiller, which has two condensers, the low condenser's heat is typically rejected to a cooling tower; therefore, it is through the low condenser that the cooling water stream from the absorber is directed. One notable difference between the integrated single-effect chiller and the integrated double-effect—other than the obvious differences, like additional components—is the split in the cooling water stream prior to its passing through the absorber. The reason for this split is discussed in detail in section 3.13. The split streams join into one stream after state point 26 and flows through the high generator, where it is further heated by a portion of the incoming exhaust gas.

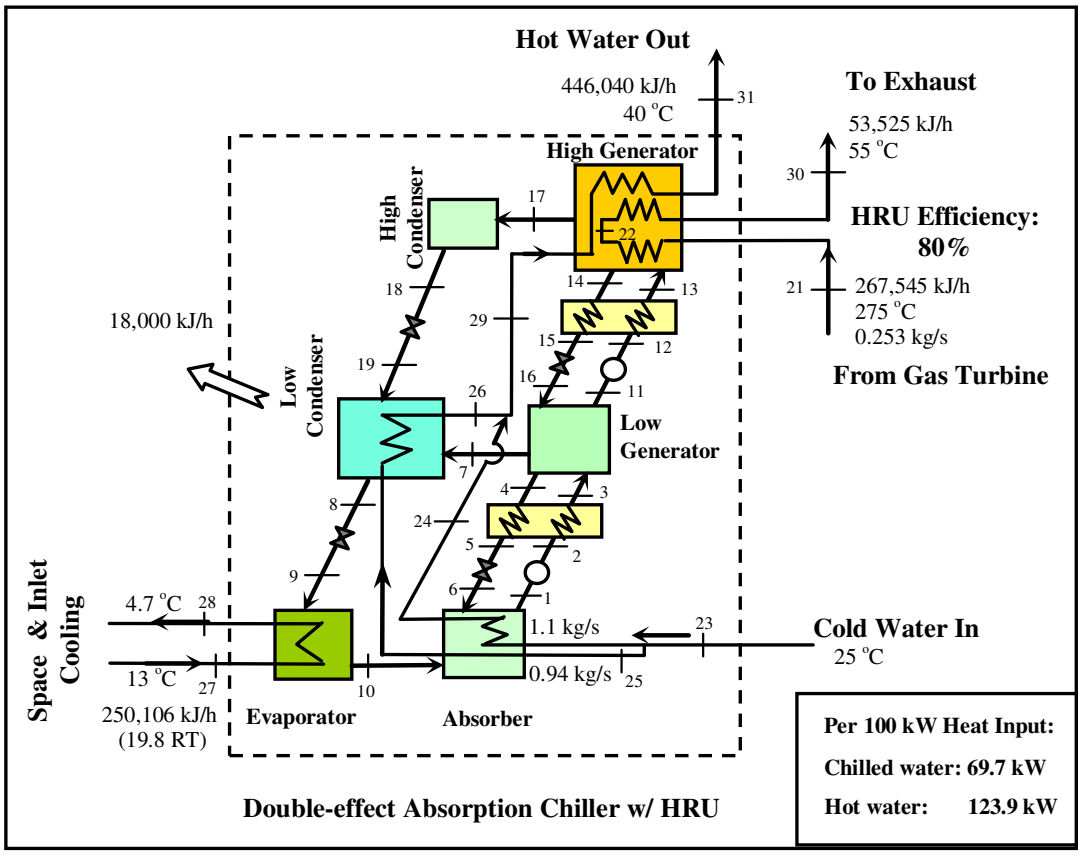

Figure 3.7 Integrated parallel-flow double-effect absorption chiller with HRU in high generator and condenser heat rejection redirected to the high generator HRU

Figure 3.8 shows the energy budget for the second design concept with the integrated double-effect absorption chiller with a COP of 1.324. Similar to the energy budget for the first design concept, 3.0 kW of chilled water from the absorption chiller is used to provide a microturbine electricity enhancement of 1.6 kW. The energy budget for the second design concept shows that the hot water production and cooling capacity of the absorption chiller increase when a double-effect chiller is employed. The hot water production increases 34% from 92.2 kW to 123.9 kW, and the chilled water production increases 91% from 34.8 kW (9.9 RT) to 66.47 kW (18.9 RT). The overall performance of design concept 2 reaches 214.9%. The total savings of this design includes 1.6 kW of electricity enhancement, 22.2 kW electricity savings to produce 66.47 kW of chilled water, and the fuel cost to produce 123.9 kW of hot water at 40°C.

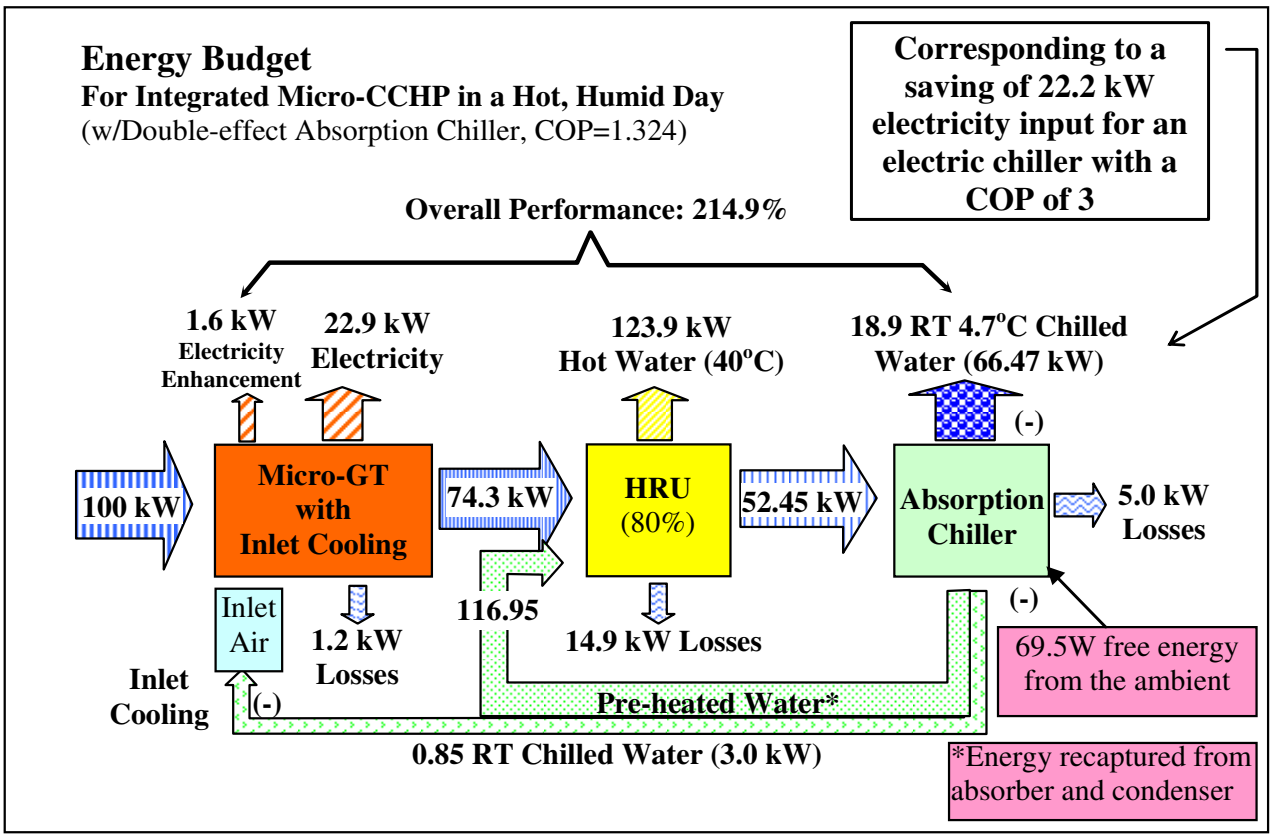

Figure 3.8 Energy budget for micro-CCHP concept design 2—integrated double-effect chiller with 100 kW (HHV) fuel input

3.5 Designs Based on the Capstone C30 Rated Fuel Input of 122.2 kW

As mentioned before, the existing micro-CCHP system (Fig. 3.1), design concept 1 (Fig. 3.5), the integrated single-effect chiller (Fig. 3.4), and the integrated double-effect chiller (Fig. 3.7) and the energy budgets (Figs. 3.2, 3.6, 3.8) for the three systems discussed are based on a fuel input of 100 kW (HHV) for convenience. However, according to the Capstone C30 spec sheet (Capstone Turbine Corporation, 2002), the rated fuel input of the microturbine is 440,000 kJ/h, or 122.2 kW. To complete the discussion of the three aforementioned micro-CCHP systems, the rated fuel input figures corresponding to those already presented are presented here. Figure 3.9 is the existing micro-CCHP system with standalone microturbine, heat recovery unit, single-effect absorption chiller, and cooling tower, and Figure 3.10 is the energy budget for it.

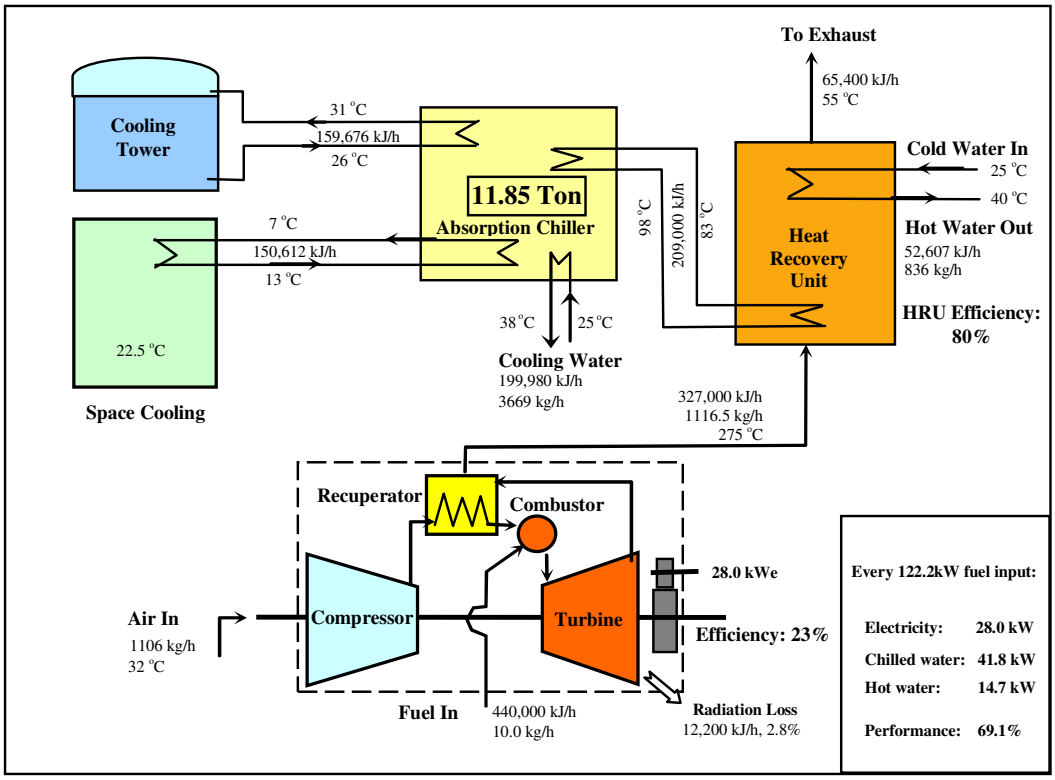

Figure 3.9 Existing micro-CCHP system based on rated fuel input of 122.2 kW (HHV)

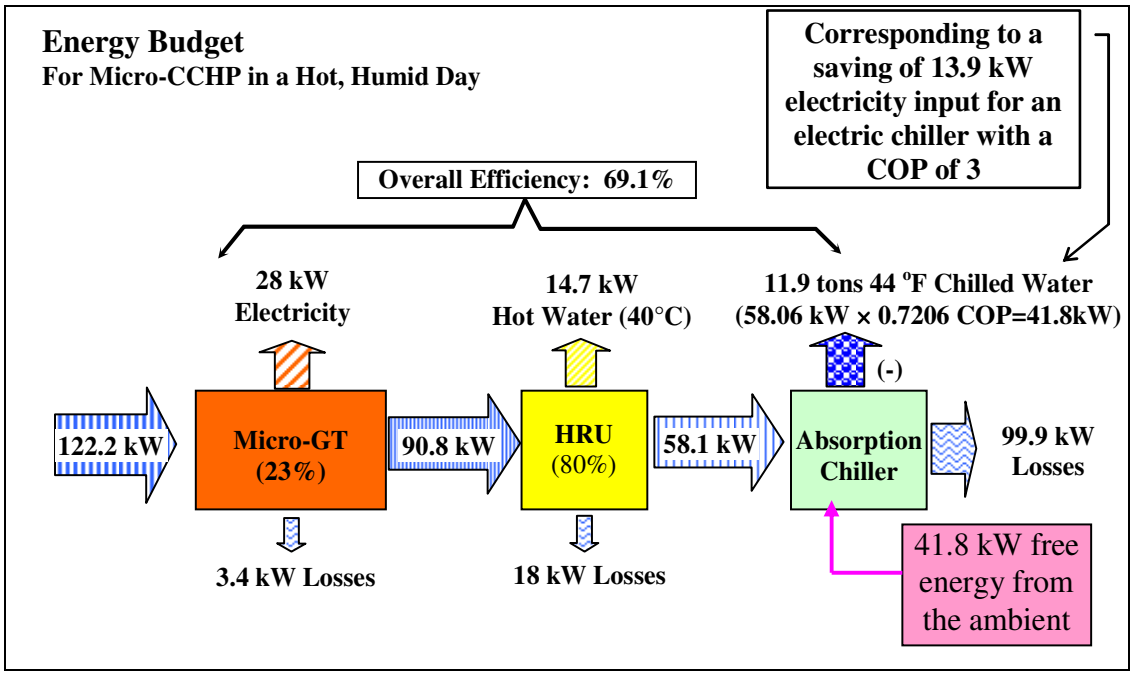

Figure 3.10 Energy budget for the existing micro-CCHP system based on rated fuel input of 122.2 kW (HHV)

Figure 3.11 is the integrated single-effect absorption chiller with the heat recovery unit in the generator and condenser heat rejection redirected to the generator HRU. This figure uses the rated microturbine exhaust energy of 327,000 kJ/h, or 90.8 kW, and the rated exhaust flow rate of 0.309 kg/s.

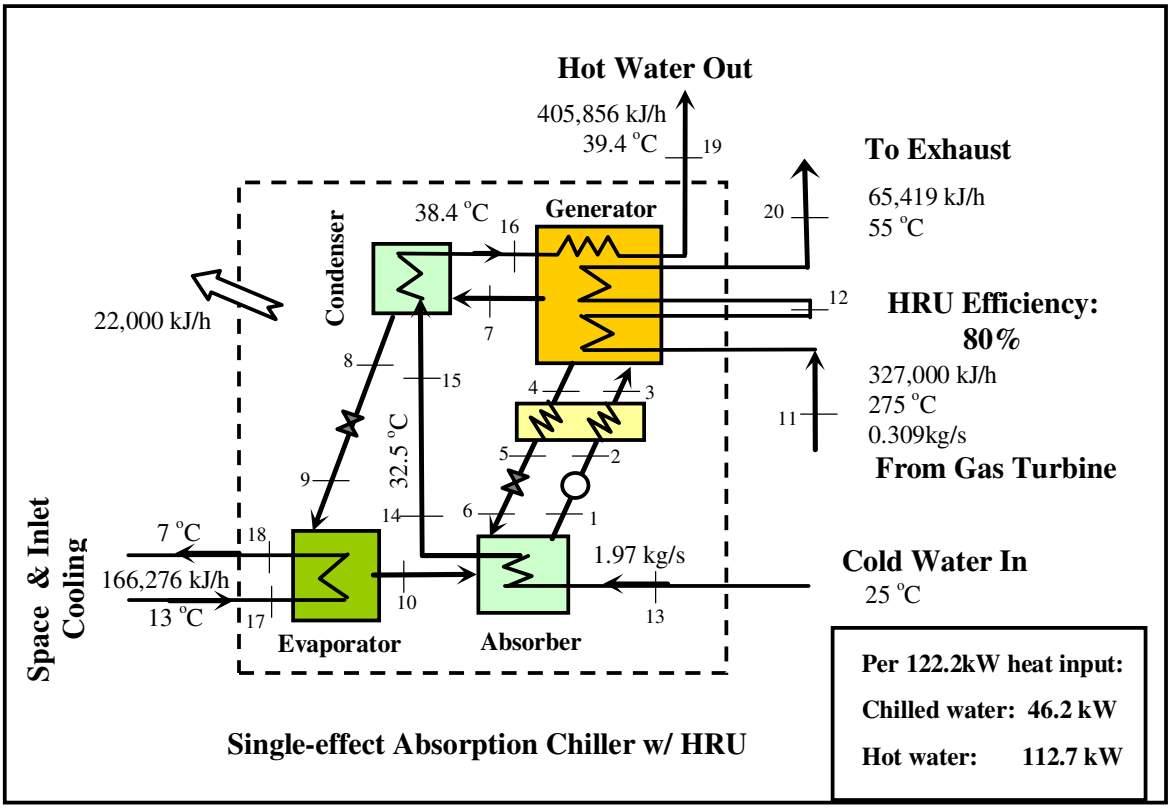

Figure 3.11 Detailed view of the integrated single-effect ACS based on the rated fuel input of 122.2 kW (HHV)

Figures 3.12 and 3.13 are the first design concept and corresponding energy budget, respectively, for the rated fuel input of 122.2 kW (HHV). Finally, Figure 3.14 is the second design concept energy budget scaled to the rated fuel input, and Figure 3.15 is the integrated double-effect absorption chiller employed in the system of the second design.

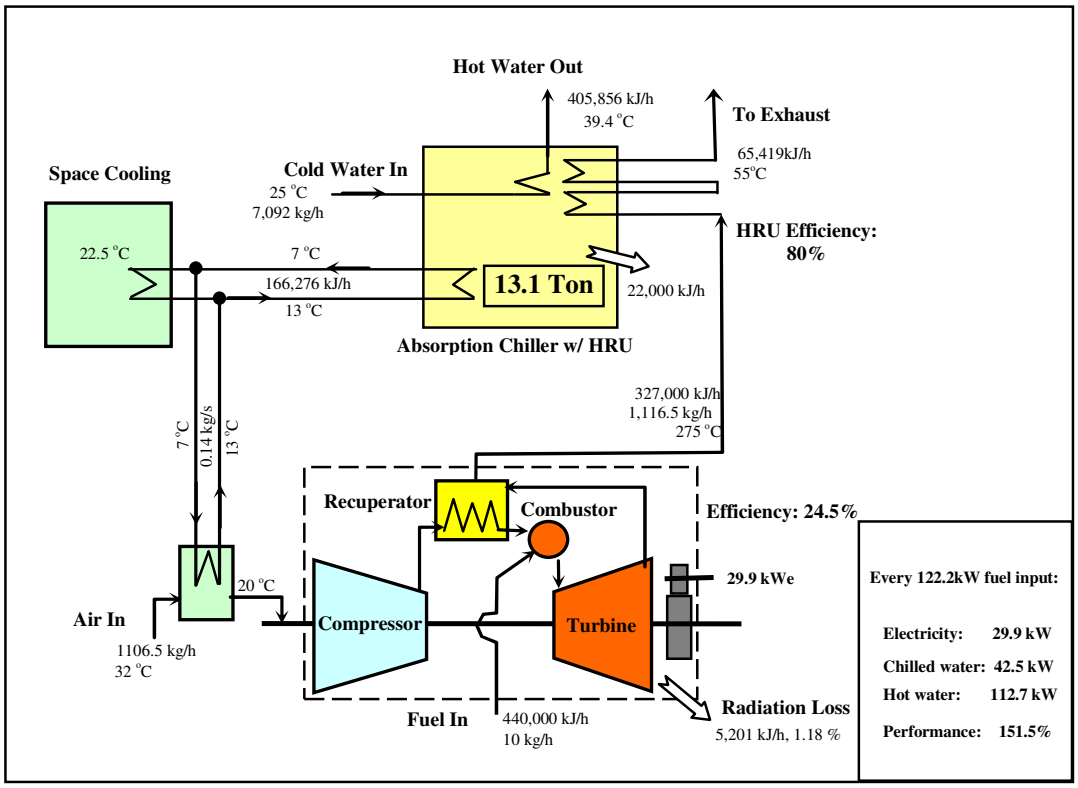

Figure 3.12 Design concept 1 with rated fuel input of 122.2 kW (HHV)

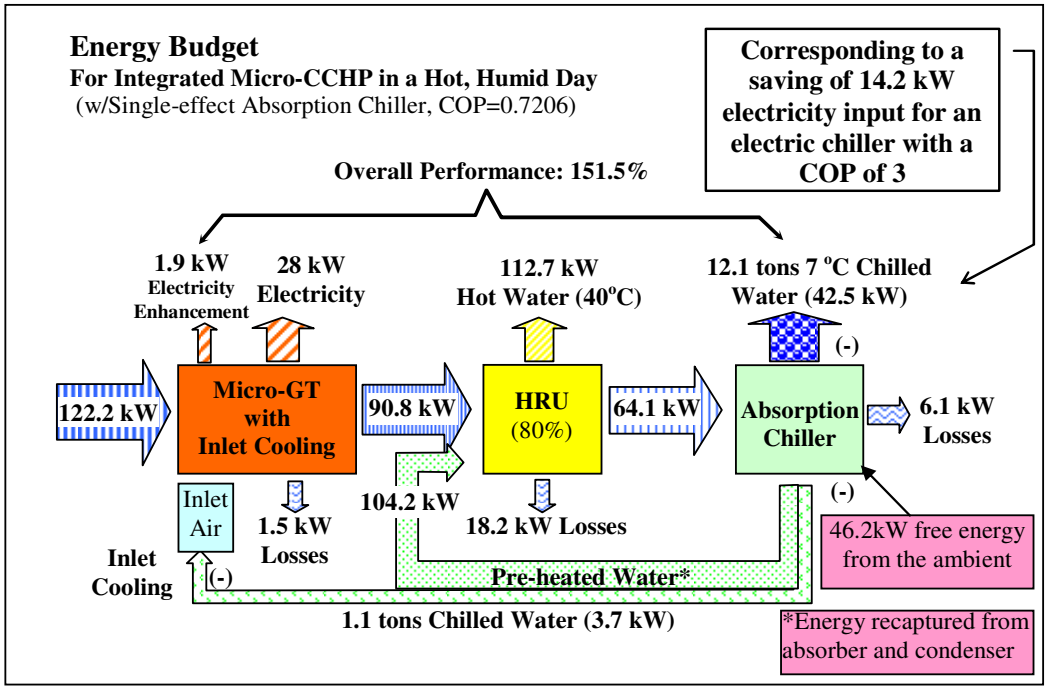

Figure 3.13 Energy budget for design concept 1 on the basis of the rated fuel input of 122.2 kW (HHV)

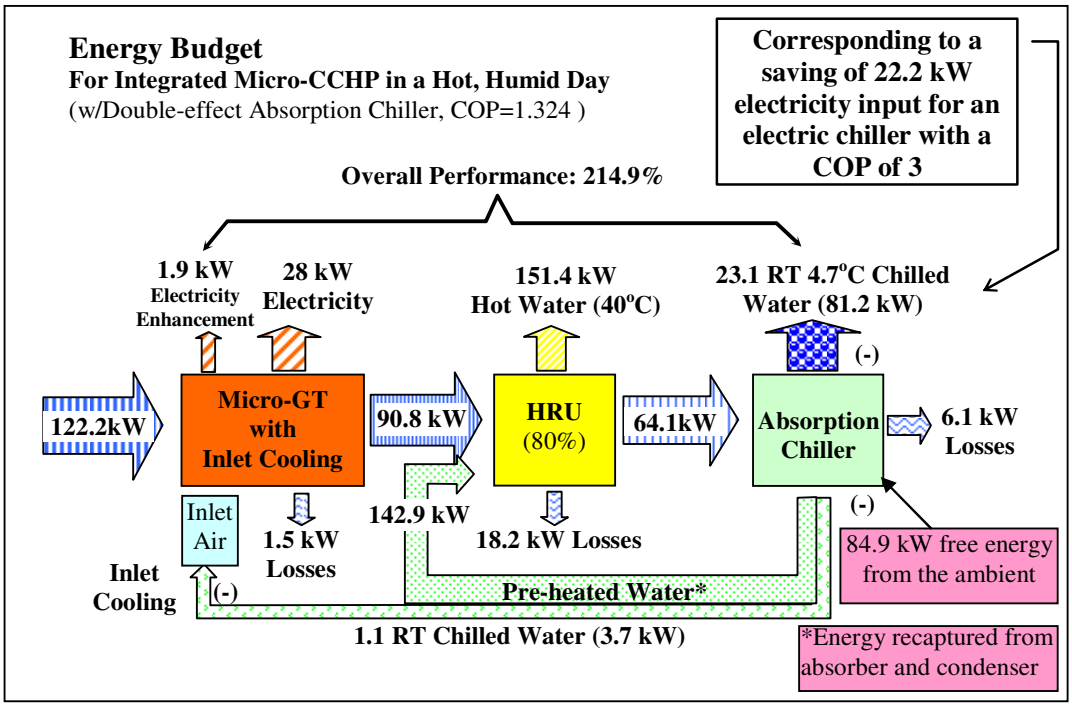

Figure 3.14 Energy budget for design concept 2 on the basis of the rated fuel input of 122.2 kW (HHV)

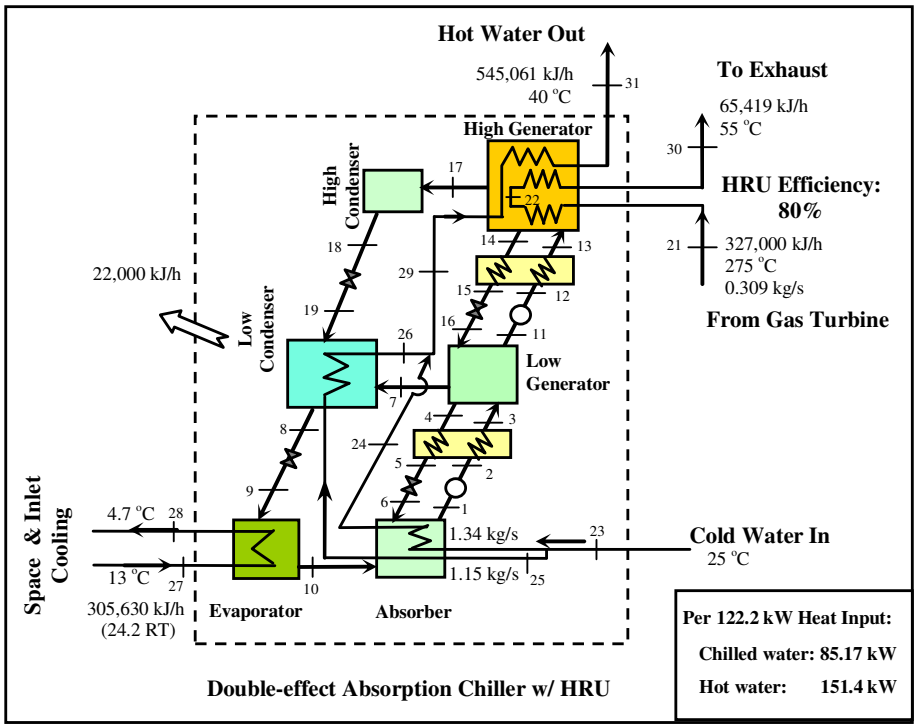

Figure 3.15 Detailed view of the integrated double-effect ACS based on the rated fuel input of 122.2 kW (HHV)

3.6 EES Computational Study of Absorption Chiller

A computational study was conducted using Engineering Equation Solver (EES) to simulate the performance of the standalone single-effect absorption chiller, the integrated single-effect chiller, and the integrated parallel-flow double-effect chiller. A parametric study was conducted for the standalone and integrated single-effect chiller to determine performance limits. Table 3.1 provides an overview of the different EES cases that will be discussed.

Table 3.1 Overview of absorption chiller cases

Case 1a	Standalone single-effect ACS, 100 kW fuel input, Q_g=47.5 kW
Case 1b	Standalone single-effect ACS, 122.2 kW fuel input, Q_g=58.1 kW
Case 2a	Integrated single-effect ACS, 100 kW fuel input, Q_g=52.45 kW
Case 2b	Integrated single-effect ACS, 122.2 kW fuel input, Q_g=64.1 kW
Case 2c	Integrated single-effect ACS, 100 kW fuel input, Q_g=59.45 kW
Case 3a	Integrated double-effect ACS, 100 kW fuel input, Q_g=52.45 kW
Case 3b	Integrated double-effect ACS, 122.2 kW fuel input, Q_g=64.1 kW
Case 3c	Integrated double-effect ACS, 100 kW fuel input, Q_g=59.45 kW

Note: Case b's are scaled up from corresponding Case a's.

Engineering Equation Solver, which provides as its basic function the numerical solution of non-linear algebraic and differential equations, is well-suited for absorption chiller system modeling because it contains built-in thermodynamic and transport property functions for lithium bromide/water and ammonia/water mixtures. Available property functions include the mixture pressure, quality (the ratio of vapor mass over liquid mass), temperature, equilibrium composition, specific enthalpy, specific entropy, specific heat capacity, density, mass fraction, mole fraction, viscosity, and thermal conductivity.

Many researchers have used EES to model and simulate absorption chiller performance. Puig-Arnavat et al. (2010) modeled both single- and double-effect lithium bromide/water absorption chillers in EES. Yin et al. (2010), Somers (2009), Figueredo et al. (2008), Yin (2006) and Herold et al. (1996) also used EES to model absorption chiller performance, from single-effect to triple-effect chillers.

3.7. Case 1a: Standalone Single-Effect Chiller, 100 kW Fuel Input, Q_g = 47.5 kW

The EES computational model developed to simulate the performance of the standalone single-effect absorption chiller used in the existing system in Figure 3.1 consists of 87 variables and 87 equations for a well-posed, solvable system. The major equations in the model are mass and energy balances for all the absorption chiller components and calls to property functions for the refrigerant water and for the lithium bromide/water solution. Table 3.2 lists the input parameters of the model. The state points in Table 3.2 refer to the state points in Figure 3.16. The major assumptions of the model are the refrigerant qualities at state points 8 and 10. *It is assumed that the refrigerant leaving the condenser is a saturated liquid (quality = 0) and that the refrigerant leaving the evaporator is saturated vapor (quality = 1.*). These assumptions are used in all cases. All of the other model inputs are design points. While it is not within the scope of this study to provide the specific design of the aforementioned components, it was verified that the design parameters in Table 3.2 are within the typical range of absorption chiller operation.

The single-effect absorption chiller model in Herold and Radermacher's *Absorption Chillers and Heat Pumps* (1996) was adapted to establish a set of reasonable inputs for the baseline case. These inputs were compared with data provided by the absorption chiller manufacturer Yazaki for its 10 TR water-fired single-effect chiller (Yazaki Energy Systems, Inc.) as well as with typical single-effect operating data in *ASHRAE Handbook 2001 Fundamentals*. Table 3.3 is the EES array of state point results for the standalone single-effect chiller baseline case.

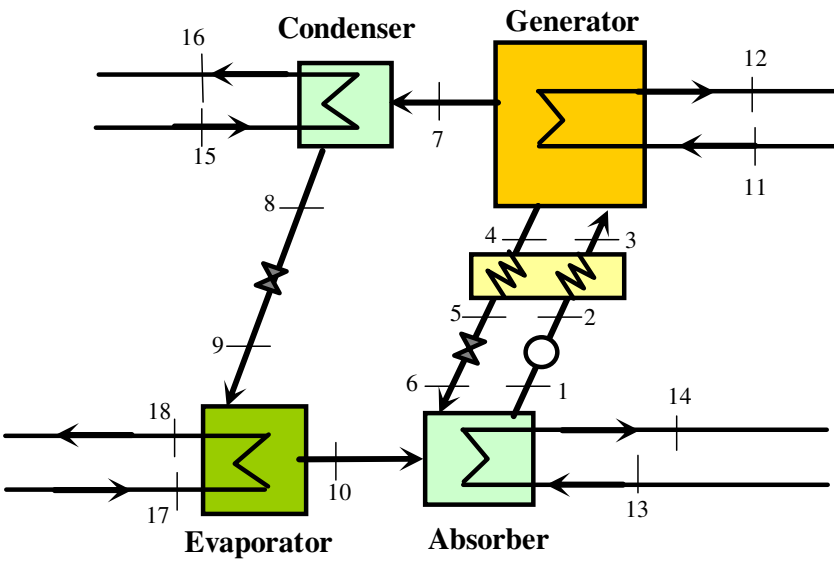

Figure 3.16 Standalone single-effect absorption chiller of Case 1a & 1b

Table 3.2 EES single-effect absorption chiller model inputs

EES Model Inputs	State Point
Solution heat exchanger effectiveness	N/A
Mass flow of dilute solution exiting absorber	1
Temperature of dilute solution exiting absorber	1
System high pressure	2,3,4,5,7,8
System low pressure	1,6,9,10
Temperature of strong solution leaving generator	4
Quality of refrigerant exiting condenser	8
Quality of refrigerant exiting evaporator	10
Temperature of absorber cooling water in external HX loop	13
Mass flow of absorber cooling water in external HX loop	13
Temperature of hot water entering generator in external HX loop	11
Mass flow of hot water entering generator in external HX loop	11
Temperature of cooling tower water entering condenser	15
Mass flow of cooling tower water entering condenser	15
Ambient temperature of water entering evaporator in external HX loop	17
Mass flow of water entering evaporator in external HX loop	17

Table 3.3 EES array of state point results for standalone single-effect absorption chiller in baseline case

	1 m_i [kg/s]	2 Q_i [Vapor Quality]	3 T_i [deg C]	4 x_i [LiBr wt. %]	5 P_i [kPa]
[1]	0.1619		32.9	56.72	0.679
[2]	0.1619		32.9	56.72	7.347
[3]	0.1619		63.2	56.72	7.347
[4]	0.1472		89.4	62.37	7.347
[5]	0.1472		53.2	62.37	7.347
[6]	0.1472		44.7	62.37	0.679
[7]	0.01465		76.8		7.347
[8]	0.01465	0	39.9		7.347
[9]	0.01465		1.5		0.679
[10]	0.01465	1	1.5		0.679
[11]	0.756		98.0		
[12]	0.756		83.0		
[13]	0.8353		25.0		
[14]	0.8353		38.0		
[15]	1.734		26.0		
[16]	1.734		31.0		
[17]	1.362		13.0		
[18]	1.362		7.0		

3.7.1 Case 1a Solution Loop

In the solution loop of the standalone single-effect ACS of Case 1a (Fig. 3.16), a dilute LiBr-water solution—56.72 wt.% LiBr—exits the absorber at state point 1 at 32.9°C, 0.679 kPa. The dilute solution is then pumped to the chiller's high pressure of 7.347 kPa. The model assumes that there are only two pressures in the chiller and that there is no heat transferred to or from the LiBr-water solution during the pumping process (i.e. adiabatic); therefore, the dilute solution exits the solution pump at state point 2 at the same temperature, 32.9°C, as state point 1. The solution now passes through the solution heat exchanger where it is preheated by the strong solution exiting the generator. For all single-effect cases, *the solution heat exchanger effectiveness was taken to be 0.64,* a conservative estimate that allows for a more compact heat exchanger and, thus, an overall smaller chiller. The dilute solution's temperature increases from 32.9°C to 63.2°C after it passes through the solution heat exchanger. The dilute solution

enters the generator where it is further heated by the driving heat input, the net energy transferred into the generator between state points 11 and 12. This driving heat input serves to vaporize the refrigerant water out of the dilute solution. In the standalone chiller, the heat input that drives the absorption cycle is passed through the generator from the heat recovery unit in an external heat exchanger loop. In all single-effect chiller EES routines in this study, the value of the net driving heat input to the generator is established by varying two inputs: the mass flow of the solution exiting the absorber at state point 1 and the temperature of the strong solution exiting the generator at state point 4, both of which vary directly with the net heat input to the generator, Q_g. In this baseline case, as detailed in the energy budget for the existing system in Figure 3.2, Q_g is 47.5 kW; the other portion of the microturbine exhaust energy is either used in producing hot water or counted as losses in the standalone heat recovery unit.

The water vaporized out of the solution in the generator exits the generator at state point 7 at 76.8°C, while a concentrated LiBr-water solution—62.37 wt. % LiBr—exits the generator at state point 4 at 89.4°C. The strong solution is then circulated back to the absorber. During its trip back to the absorber, this strong solution transfers heat to the dilute solution in the solution heat exchanger, and its temperature drops to 53.2°C at state point 5, the exit of the solution heat exchanger. The solution then passes through an expansion valve with some water flashing to vapor, and its temperature and pressure decrease to 44.7°C and 0.679 kPa, respectively, at state point 6. Finally, the strong solution enters the absorber where it exothermically (releasing heat) absorbs the refrigerant water vapor exiting the evaporator.

3.7.2 Case 1a Refrigerant Loop

In the refrigerant loop, the refrigerant water vapor exiting the generator at 76.8°C passes through the condenser where it is cooled via two heat transfer processes, both of which are assumed isobaric at the ACS high pressure of 7.347 kPa. First, the refrigerant water is cooled from superheated vapor at 76.81°C to saturated water vapor at 39.9°C. Second, the saturated water vapor condenses to saturate liquid water at 39.9°C, releasing the latent heat. The total released heat is carried to a cooling tower and dumped to the ambient via the

external heat exchanger loop represented by state points 15 and 16.The refrigerant water leaves the condenser, as assumed, as a saturated liquid at 39.9°F. It then throttled through the refrigerant expansion valve, where its pressure is reduced to the ACS low pressure of 0.679 kPa and its temperature decreases to the system low of 1.5°C at state point 9. At this low pressure, the refrigerant flashes into the vapor phase in the evaporator, absorbing latent heat. The net value of the heat absorbed by the refrigerant in the evaporator can be obtained by using the water stream data at state points 17 and 18 in the first law of thermodynamics as in Equation 3.1:

$$Q_e = m_{17} c_{H_2O(liq)} (T_{17} - T_{18}) \qquad \text{Eqn. 3.1}$$

Where Q_e is the net heat absorbed by the refrigerant as it passes through the evaporator, m_{17} is the mass flow rate of the water in the external heat exchanger loop, $c_{H2O(liq)}$ is the specific heat of liquid water, and T_{17} and T_{18} are the temperatures of the water in the external heat exchanger loop at state points 17 and 18, respectively. The net value of the heat absorbed by the refrigerant in the evaporator can also be obtained by multiplying the mass flow rate of the refrigerant by the difference in the enthalpies at state points 9 and 10 (i.e., the latent heat). The refrigerant exits the evaporator at state point 10, as assumed, as saturated water vapor at a temperature of 1.5°C, having gained no sensible heat. Finally, the refrigerant vapor enters the absorber and is absorbed into the strong lithium bromide-water solution in an endothermic process. It then circulates in the solution loop of the absorption chiller and undergoes the same cycle again. Table 3.4 contains the net heat transfer rates in the different ACS components.

Table 3.4 Net heat transfer rates in absorption chiller components for Case 1a

Component	Variable	Net Heat Transfer Rate (kW)
Generator	Q_g	**47.50**
Absorber	Q_a	**45.45**
Condenser	Q_c	**36.29**
Evaporator	Q_e	**34.23 (9.73 RT)**

The COP of the single-effect chiller in the baseline case is 0.7206. In reality, due to irreversibilities within the chiller, the COP of a single-effect absorption chiller will rarely exceed

0.7. Theoretically, as in this EES study, the COP can be higher than 0.7. The reason for this is that the EES routine developed to model single-effect and double-effect ACS performance is a lower order model that does not account for irreversibilities, though they are accounted for as lumped losses in the overall micro-CCHP system models that the chillers are used in.

3.8 Case 1b: Standalone Single-Effect ACS, 122.2 kW Fuel Input, Q_g=58.1kW

Case 1b is derived from Case 1a by scaling up the mass flow rates of Case 1a to account for the actual rated fuel input of 122.2 kW. The result is that the net energy transferred into or out of the absorption chiller's components is also scaled up. The standalone chiller in Figure 3.9 is the chiller in this case. Table 3.5 contains the net heat transfer rates in the different ACS components for Case 1b. The COP of the chiller in this case is 0.7206, the same as in Case 1a, because Q_g and Q_e scaled up proportionally.

Table 3.5 Net heat transfer rates in absorption chiller components for Case 1b

Component	Variable	Net Heat Transfer Rate (kW)
Generator	Q_g	58.05
Absorber	Q_a	55.55
Condenser	Q_c	44.35
Evaporator	Q_e	41.80 (11.89 RT)

3.9 Case 2a: Integrated Single-Effect ACS, 100 kW Fuel Input, Q_g=52.45kW

Once the baseline model in Case 1a was validated with existing data, the baseline EES routine was modified to simulate the performance of the integrated chiller in Figure 3.4. The EES computational model developed to simulate the performance of the integrated single-effect absorption chiller *consists of 94 variables and 94 equations* for a well-posed, solvable system. The additional equations account for the integration of the cooling tower function into the condenser and of the heat recovery unit into the generator and for the addition of the hot water production line. Additional property calls were also required. Table 3.6 lists the inputs for the integrated single-effect chiller model. The state points in Table 3.6 refer to the state points in Figure 3.17. Except for the assumptions about the vapor quality of the refrigerant at state

points 8 and 10, all of the other model inputs are design points that the prospective manufacturer of the integrated single-effect chiller will achieve by varying chiller hardware parameters, such as the size and type of internal heat exchangers, the size of cooling water pumps, and the size of internal piping.

Many of the inputs for the integrated single-effect chiller model are the same as for the standalone model with some major exceptions. Since the cooling tower has been eliminated and the absorber cooling water stream is now used to cool the condenser, there is no longer an external heat exchanger loop passing through the condenser; therefore, the temperature and mass flow rate of the condenser cooling water at state point 15 no longer need to be specified. Instead, the temperature and mass flow rate at that point are linked to the temperature and mass flow rate at state point 14. Another difference between the inputs for the standalone single-effect chiller and the integrated chiller in this case is the input specification of how much of the microturbine's exhaust energy entering the generator HRU is dedicated to hot water production.

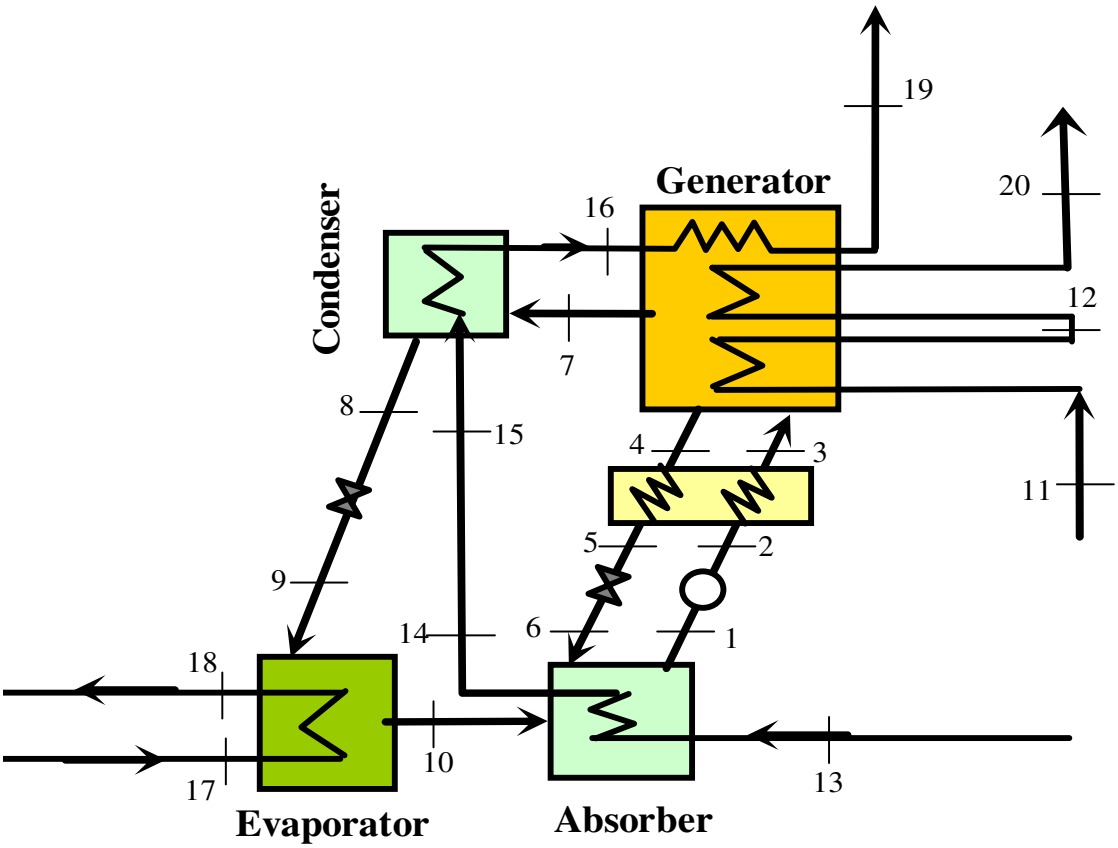

Figure 3.17 **Integrated single-effect absorption chiller of Case 2a, 2b, & 2c**

Table 3.6 EES integrated single-effect absorption chiller model inputs

EES Model Inputs	State Point
Solution heat exchanger effectiveness	N/A
Mass flow of dilute solution exiting absorber	1
Temperature of dilute solution exiting absorber	1
System high pressure	2,3,4,5,7,8
System low pressure	1,6,9,10
Temperature of strong solution leaving generator	4
Quality of refrigerant exiting condenser	8
Quality of refrigerant exiting evaporator	10
Temperature of absorber cooling water	13
Mass flow of absorber cooling water	13
Temperature of microturbine exhaust entering generator HRU	11
Mass flow of microturbine exhaust entering generator HRU	11
Ambient temperature of water entering evaporator in external HX loop	17
Mass flow of water entering evaporator in external HX loop	17
Portion of microturbine exhaust used in HRU hot water production (Q_{hw})	N/A

Table 3.7 is the EES array of state point results for the integrated single-effect chiller in Case 2a. The temperatures, pressures, enthalpies, and LiBr concentrations for state points 1-10 are identical to those of the standalone chiller in Case 1a. Similarly, the processes and phase changes in the solution loop and refrigerant loop are the same.

The major differences between Case 1a and this case result from the integration of the heat recovery unit into the generator and the integration of the cooling tower function into the condenser of the absorption chiller cycle. First, due to the fact that the heat recovery unit has been integrated into the generator, the net driving heat input to the generator (Q_g) has increased from 47.5 kW in Case 1a to 52.45 kW. To model this increase in generator input for the particular equations used in EES, it was necessary to increase the input mass flow rate of the dilute solution exiting the absorber. Increasing the mass flow rate of the solution at state point 1 caused an increase in the mass flow rates at all the state points in the solution loop and in the refrigerant loop. With the temperatures and pressures the same as in Case 1a, this increase in solution and refrigerant flow rates results in an increase in the net heat transfer rates of the chiller's components. Also due to HRU integration, the microturbine exhaust, which

is modeled in EES as N_2, transfers heat directly to the generator. According to Capstone C30 specifications, the exhaust (state point 11) is at a temperature of 275°C and is available with a mass flow rate of 0.253 kg/s for 100 kW of fuel input. As can be seen in Table 3.7, the temperature and mass flow rate input at state point 11 has been adjusted to reflect the microturbine specifications. The property call to calculate the enthalpy of the fluid at state points 11 and 12 also had to be adjusted to reflect the change from water in Case 1a to nitrogen gas in this case. It is assumed that the exhaust does not undergo a pressure or temperature drop between the exit of the microturbine and the inlet of the generator HRU.

Second, the integration of the HRU into the generator enables hot water production directly from the absorption chiller, rather than from the standalone HRU, as in Case 1a. Assuming a generator HRU efficiency of 80%, for 100 kW of fuel input, the total microturbine exhaust energy available to the generator HRU is 59.45 kW. Of that 59.45 kW, after 52.45 kW of energy is transferred to the generator as the cycle's driving input, 7.0 kW of energy is dedicated to hot water production. In Figure 3.17, this 7.0 kW of energy is transferred from the exhaust between state points 12 and 20 to the hot water line between state points 16 and 19, increasing the temperature of the hot water from 38.4°C to 39.4°C. This is a very small temperature change, but the focus of this study is the cooling capacity of the absorption chiller, not hot water production. Should more hot water be required, the design of the chiller could be altered to achieve this.

Table 3.7 EES array of state point results for integrated single-effect absorption chiller in Case 2a

	1 m_i [kg/s]	2 Q_i [Vapor Quality]	3 T_i [deg C]	4 x_i [LiBr wt. %]	5 P_i [kPa]
[1]	0.1787		32.9	56.72	0.679
[2]	0.1787		32.9	56.72	7.347
[3]	0.1787		63.2	56.72	7.347
[4]	0.1626		89.4	62.37	7.347
[5]	0.1626		53.2	62.37	7.347
[6]	0.1626		44.7	62.37	0.679
[7]	0.01618		76.8		7.347
[8]	0.01618	0	39.9		7.347
[9]	0.01618		1.5		0.679
[10]	0.01618	1	1.5		0.679
[11]	0.253		275.0		
[12]	0.253		80.4		
[13]	1.61		25.0		
[14]	1.61		32.4		
[15]	1.61		32.4		
[16]	1.61		38.4		
[17]	1.505		13.0		
[18]	1.505		7.0		
[19]	1.61		39.4		
[20]	0.253		54.4		

Third, due to the fact that the cooling tower function has been integrated into the condenser of the absorption chiller cycle, the cooling water line from the cooling tower— the line through state points 15 and 16—is now connected to the absorber cooling water line. In connecting these lines, it is necessary to adjust the mass flow rate of the absorber cooling water in order to ensure that the second law of thermodynamics is not violated. The two temperature restrictions that limit the mass flow rate of the absorber cooling water are (1) that the temperature of the cooling water at the exit of the absorber, state point 14, cannot be greater than the temperature of the strong solution entering the absorber at state point 6 (44.7°C) and (2) that the temperature of the cooling water between state points 14 and 16 (not just at the one point of 14) must be lower than the condenser temperature of 39.9°C in order to provide condenser cooling. It was determined that a mass flow rate of 1.61 kg/s enables the absorber cooling water stream to fulfill both requirements.

The reason for the second constraint listed above is that, in the EES model, the condenser heat exchanger has a twofold function, as shown in Figure 3.18: it is both a cooler and a condenser. The superheated water vapor at state point 7 enters the condenser heat exchanger at 76.8°C and is first cooled to saturated water vapor at 39.9°C—i.e., the sensible heat of the superheated refrigerant vapor at state point 7 is transferred to the cooling water stream coming from the absorber (state point 15). Next, the saturated water vapor of 39.9°C (state point 7a in Fig. 3.18) condenses, transferring its latent heat to the cooling water stream, to saturated liquid water at the same temperature (39.9°C) and exits the condenser heat exchanger at this temperature at state point 8. Therefore, the temperature of the condenser cooling water at state point 15 must be low enough to provide cooling for both processes in the condenser heat exchanger during the entire isothermal condensation process. Another constraint on the temperature of the cooling water at state point 15 is that a finite approach temperature must be maintained between the refrigerant temperature (state point 8) at the exit of the condenser heat exchanger and the cooling water temperature (state point 15) at the inlet of the cooler section of the exchanger. Figure 3.19 illustrates this point. A 7.5°C pinchpoint has been used here. There was a temptation to use less cooling water to save water consumption as well as to boost the temperature of the hot water output from the micro-CCHP system. If 40% less cooling water were used, there would be sufficient cooling capacity to absorb all the heat dumped from the refrigerant (based on the thermodynamics first law), but the cooling water temperature (shown as the dashed blue curve in Figure 3.19) would have become higher than the condensation temperature halfway through the condensation process, which would be a violation of the thermodynamic second law. Use of a higher flow rate reduces the temperature of the hot water output from approximately 60°C to 40°C, but with 40% more available flow rate.

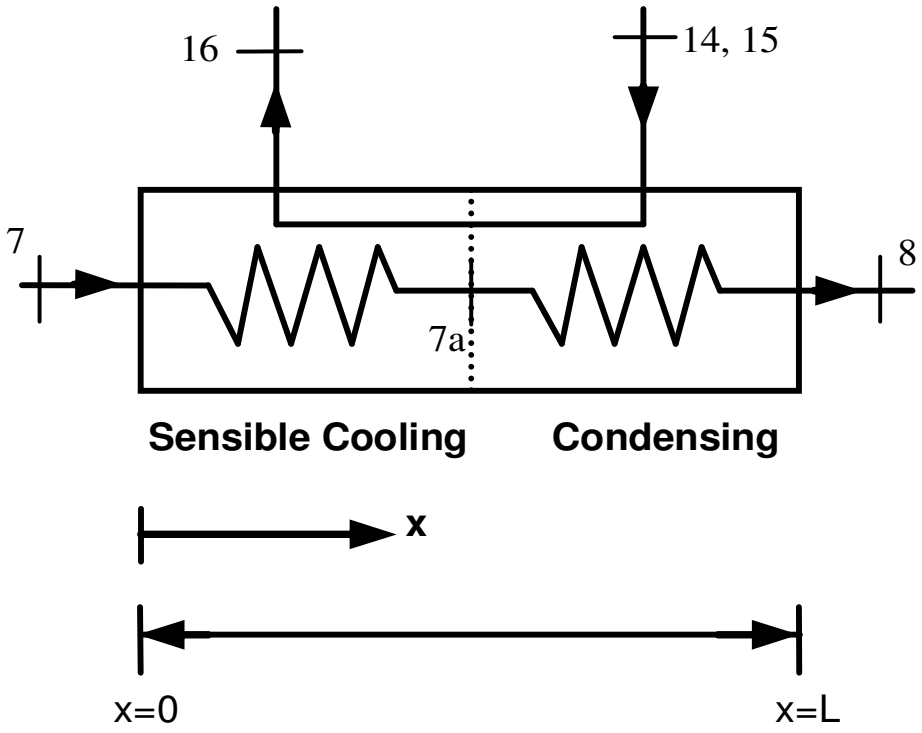

Figure 3.18 Dual function of condenser heat exchanger

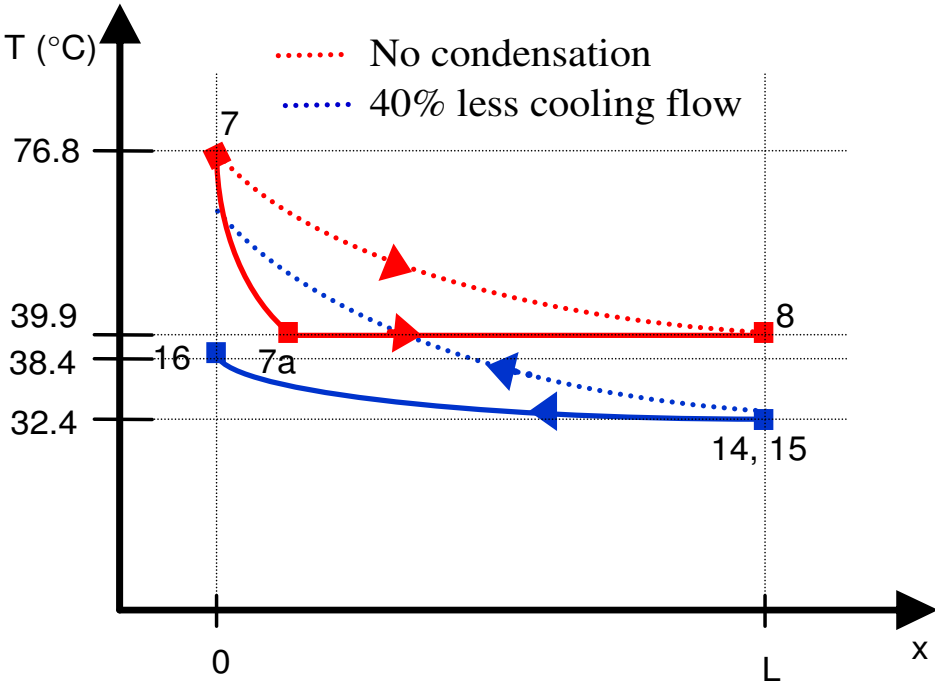

Figure 3.19 Temperature vs. distance for condenser heat exchanger

Table 3.8 contains the net heat transfer rates in the different ACS components. Even though Q_g and Q_e increased here from their values in Case 1a, their increase is proportional; therefore, the COP of the integrated single-effect chiller in this case is 0.7206, the same as in Case 1a.

Table 3.8 Net heat transfer rates in integrated absorption chiller components for Case 2a

Component	Variable	Net Heat Transfer Rate (kW)
Generator	Q_g	**52.45**
Absorber	Q_a	**50.18**
Condenser	Q_c	**40.06**
Evaporator	Q_e	**37.79 (10.75 RT)**

3.10 Case 2b: Integrated Single-Effect ACS, 122.2 kW Fuel Input,Q_g=64.1kW

Case 2b is derived from Case 2a by scaling up the mass flow rates of Case 2a to account for the actual rated fuel input of 122.2 kW. The result is that the net energy transferred into or out of the absorption chiller's components is also scaled up. The integrated chiller in Figure 3.11 is the chiller in this case. Table 3.9 contains the net heat transfer rates in the different ACS components for Case 2b. The COP of the chiller in this case is 0.7206, the same as in Case 2a, because Q_g and Q_e scaled up proportionally.

Table 3.9 Net heat transfer rates in absorption chiller components for Case 1b

Component	Variable	Net Heat Transfer Rate (kW)
Generator	Q_g	**64.09**
Absorber	Q_a	**61.32**
Condenser	Q_c	**48.95**
Evaporator	Q_e	**46.18 (13.13 RT)**

3.11 Integrated Single-Effect ACS Parametric Study

After the integrated chiller of Case 2a was modeled in EES, the calculation routine was used to simulate the performance of the chiller in Figure 3.17 for different design cases. The main objective in each simulation from case to case is to maximize the absorption chiller's cooling capacity by increasing the temperature in the generator. In the EES model, to increase the temperature in the generator without involving a detailed heat exchanger design or assumptions about the size of the generator heat exchanger, the temperature at state point 4 was increased; and with it, the mass flow rate of the dilute solution exiting the absorber at state point 1 was adjusted to maintain the desired Q_g. Adjustment of the dilute solution will proportionally adjust both the refrigerant and the solution flow rate, keeping the concentration identical at 56.72%. The input parameters in Table 3.6 were varied to determine what combination of inputs produces the highest COP for the integrated chiller.

3.12 Case 2c: Integrated Single-Effect ACS, 100 kW Fuel Input, Q_g=59.45kW (Seeking a Smaller ACS)

The design of the ACS in earlier cases was based on the heat source temperature ranging from 100 to 150 ^{o}C. Since the hot exhaust gas at 275^{o}C from a microturbine is to be directly employed in the ACS's generator, it becomes of interest to investigate how this higher grade energy can be harvested. Four advantages are identified: (a) at the same heating rate, a higher temperature difference between the heat source and the strong LiBr solution can reduce the heat exchanger size in the generator; (b) with the same heat exchanger size, more heat can be transferred and more cooling can be achieved; (c) with the same heat exchanger size and same heating rate, the steam can be generated at a higher pressure and, hence, the ACS's COP can be increased; (d) the temperature of the strong LiBr solution can be increased to reduce its flow rate, so a smaller ACS can be used. Considering one of the important objectives of this study is to make a compact system, in the following Case 2c, the focus is therefore placed on item (d) to investigate how much the LiBr flow rate can be reduced before the solution stops performing properly.

The optimization process is made by iterating back and forth between the strong LiBr solution's temperature (T4) and the heat input (Q_g). Both the high and low pressures in the system are also fixed. The constraint is imposed by the concentration of the LiBr strong solution. The iteration process is documented in Appendix C.

At a fixed high pressure of 7.347 kPa and a fixed low pressure of 0.679 kPa, the temperature of the solution at the generator exit cannot be increased beyond 143.6°C in the EES model. Beyond this temperature, the EES solution for the LiBr concentration at state point 4 will not converge due to the uncertainty in interpolating the property table of LiBr in EES routine. Increasing the chiller's high pressure allows the temperature at state point 4 to be increased incrementally, but increasing the high pressure also causes the COP of the chiller to decrease. The decrease in COP because of an increase in the system's high pressure occurs because less refrigerant water vaporizes from the solution in the generator at a higher pressure, which results in a reduction in the refrigerant flow rate in the chiller's refrigerant loop, a decrease in the net heat transfer into the evaporator, and, thus, a reduction in the chiller's cooling capacity. This is why the parametric study was undertaken by fixing the high pressure value.

The result shows that for a fixed Q_g, high pressure, and low pressure in the system, increasing the temperature of the strong solution at the exit of the generator (state point 4) results in an increase in chiller cooling capacity and, thus, an increase in the COP of the chiller. As the temperature in the generator increases, as expected, the mass flow rate of the LiBr-water solution in the solution loop of the chiller can be decreased to receive the entire heat load. The reason that COP increases is that, as the generator temperature increases, a greater percentage of refrigerant water is vaporized from the LiBr-water solution in the generator. This leaves a strong solution with a higher LiBr concentration. Because LiBr is a salt, as the concentration of LiBr increases, the solution becomes thick.

The EES model input parameters were varied to determine the combination that results in a solution that converges and yields the highest chiller COP. In this way, the limits of the integrated single-effect model were determined. Case 2c presents the highest theoretical COP

and the lowest flow rate of LiBr-water solution that can be obtained for the integrated single-effect chiller based on the design constraints and considerations of this study.

In this case, to achieve the greatest evaporator cooling capacity, the net heat transfer from the microturbine exhaust to the generator was maintained at 59.45 kW. Therefore, none of the recovered exhaust energy is used to augment hot water production. Table 3.10 contains the EES array of state point results for this case. The temperature of the strong solution at state point 4 is set to 143.6°C, the highest temperature for which the solution converges. The resulting COP of the chiller in this case is 0.784, the highest theoretical COP that could be obtained for a single-effect chiller using the EES model. While the COP is very good for a single-effect chiller, an examination of the state point results reveals some anomalies and potential issues.

In Case 2c the mass flow rate of the refrigerant water has increased, but the mass flow rate of the dilute solution at state points 1, 2, and 3 has decreased by 63% compared to case 2a. The mass flow rate of the strong solution at state points 4, 5, and 6 has a greater decrease of 72% compared to Case 2a. With this significant reduction of mass flow, the LiBr concentration is extremely high at 81.39%. Reliable property data for LiBr does not exist beyond concentrations of 75%. In version 6 of EES used in this study, the properties of LiBr are valid only up to concentrations of 70%. The most recent versions have updated the LiBr database to reflect the property relations set forth in Patek and Klomfar [reference] in 2006, which are valid for temperatures up to 500 K and concentrations up to 75%. Nonetheless, the strong solution has too much lithium bromide in it, becoming too thick with the salt. The thickness of the solution poses additional problems, such as the increased viscosity with associated larger pressure drop and increased likelihood of corrosion in the chiller tubing as the hot, sludgy solution crawls through it. Therefore, Case 2c serves only as an exploratory case in this study; and in the remaining cases in this study, the temperature of T4 and LiBr solution flow rate of the baseline, Case 2a, will be used.

Table 3.10 EES array of state point results for integrated single-effect absorption chiller in Case 2c

	1 m_i [kg/s]	2 Q_i [Vapor Quality]	3 T_i [deg C]	4 x_i [LiBr wt. %]	5 P_i [kPa]
[1]	0.06584		32.9	56.72	0.679
[2]	0.06584		32.9	56.72	7.347
[3]	0.06584		76.4	56.72	7.347
[4]	0.04589		143.6	81.39	7.347
[5]	0.04589		72.8	81.39	7.347
[6]	0.04589		77.8	81.39	0.679
[7]	0.01995		76.8		7.347
[8]	0.01995	0	39.9		7.347
[9]	0.01995		1.5		0.679
[10]	0.01995	1	1.5		0.679
[11]	0.253		275.0		
[12]	0.253		54.3		
[13]	1.61		25.0		
[14]	1.61		33.4		
[15]	1.61		33.4		
[16]	1.61		40.7		
[17]	1.505		13.0		
[18]	1.505		5.6		
[19]	1.61		40.7		
[20]	0.253		54.3		

Another issue with the state point results can be seen with the temperature of state points 5 and 6. In an expansion process, the temperature and pressure of a fluid is supposed to decrease. Here, the temperature of the strong solution increases in the solution expansion valve. This could be a result of an inversion point caused by the Joule-Thompson effect, but because property data does not exist for lithium bromide-water solutions with an LiBr concentration of 81.39%, it cannot be ascertained whether the temperature increase of the solution is a result of the Joule-Thompson effect or a result of unreliable property data. Regardless, the temperature of the solution at state point 6 is too high. Such a high temperature solution will increase the heat load of the absorber, requiring additional cooling so that the refrigerant vapor entering the absorber from the evaporator will dissolve completely in the absorbent solution.

It is interesting to note that, even though no portion of the microturbine exhaust is used to augment the production of hot water, the hot water outlet temperature has increased 1.3°C from 39.4°C in case 2a to 40.7°C in this case. This temperature increase is a result of an increase in the heat transferred from the absorber and condenser to the hot water line, as can be seen in Table 3.11 below.

Table 3.11 Net heat transfer rates in absorption chiller components for Case 2c

Component	Variable	Net Heat Transfer Rate (kW)
Generator	Q_g	**59.45**
Absorber	Q_a	**56.66**
Condenser	Q_c	**49.40**
Evaporator	Q_e	**46.61 (13.25 RT)**

In light of the issues raised in this single-effect limiting case, it is determined that a double-effect absorption chiller should be used in the micro-CCHP system in order to maximize the overall thermal performance of the system. Double-effect chillers have the capacity to make better use of high temperature exhaust gas, and their coefficients of performance tend to be around 1.3. This equates to a sizeable increase in cooling capacity, as will be seen in the discussion of the integrated double-effect chiller in the next section.

3.13 Case 3a: Integrated Double-Effect ACS, 100 kW Fuel Input, Q_g=52.45kW

As discussed in [Case 1a section], the EES models discussed in this study assume that the absorption cycle is reversible. This assumption allows the COP of the single-effect chillers to reach values of 0.784, as in the last case; however, in a real single-effect chiller, losses due to irreversibilities usually do not permit the COP of the device to exceed 0.7. In this case, a double-effect absorption chiller is used to take advantage of the high temperature exhaust heat, thereby increasing the chilled water production for the same driving heat input—Q_g = 52.45 kW—as in Case 2a. Figure 3.20 is the schematic of the integrated parallel flow double-effect absorption chiller used in this case.

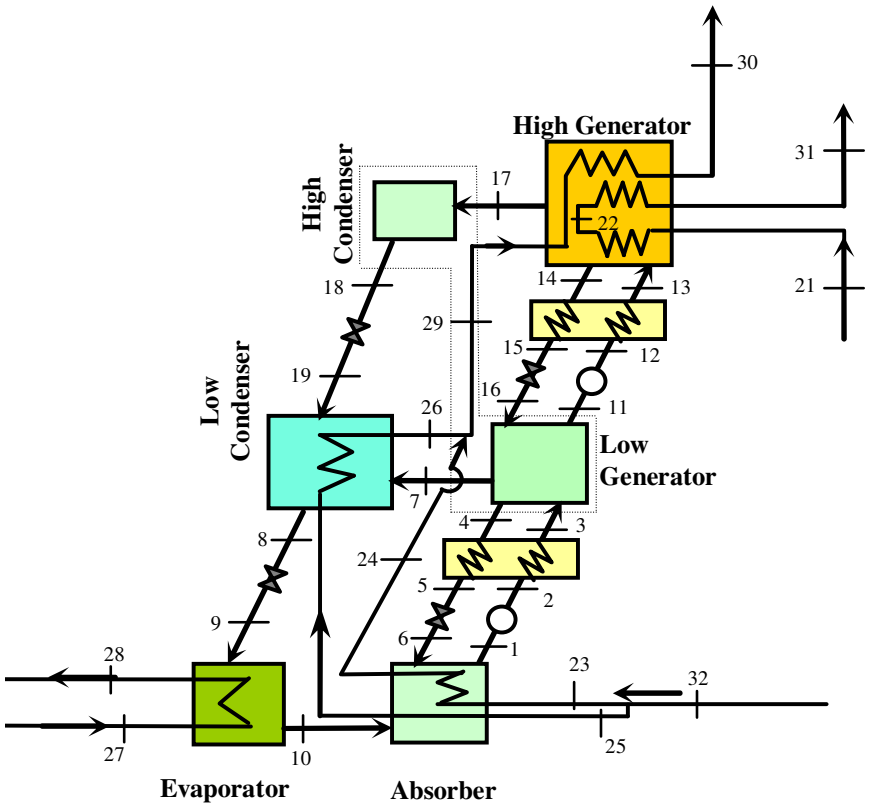

Figure 3.20 Integrated parallel-flow double-effect absorption chiller of Cases 3a & 3b

The EES model developed for the integrated *double-effect chiller consists of 154 equations*. The additional equations account for essentially what is like modeling two single-effect chillers in one. Hence, the number of equations used in this case is nearly twice that of the standalone single-effect chiller cases. Table 3.12 lists the inputs for the integrated double-effect EES model, and Table 3.13 is the array of state point results for the double-effect chiller of this case. State point 20 is not used in the state point numbering scheme for this case.

Table 3.12 EES integrated double-effect absorption chiller model inputs

EES Model Inputs	State Point
Solution heat exchanger effectiveness	N/A
Mass flow of dilute solution exiting absorber	1
Temperature of dilute solution exiting absorber	1
System high pressure	12,13,14,15,17,18
System intermediate pressure	2,3,4,5,7,8,11,16,19
System low pressure	1,6,9,10
Temperature of strong solution exiting generator	4
Quality of refrigerant exiting condenser	8
Quality of refrigerant exiting evaporator	10
Temperature of solution exiting low generator	11
Temperature of solution exiting high generator	14
Temperature of absorber cooling water	23
Mass flow of absorber cooling water	23
Temperature of low condenser cooling water	25
Mass flow of low condenser cooling water	25
Temperature of microturbine exhaust entering generator HRU	21
Mass flow of microturbine exhaust entering generator HRU	21
Ambient temperature of water entering evaporator in external HX loop	27
Mass flow of water entering evaporator in external HX loop	27
Portion of microturbine exhaust used in HRU hot water production (Q_{hw})	N/A

Table 3.13 EES array of state point results for integrated double-effect absorption chiller in Case 3a

	1 m_i [kg/s]	2 q_i [Vapor Quality]	3 T_i [deg C]	4 x_i [LiBr wt. %]	5 P_i [kPa]
[1]	0.1962	0	29.9	52.8	0.88
[2]	0.1962		29.9	52.8	4.171
[3]	0.1962		47.3	52.8	4.171
[4]	0.1671	0	76.4	62.0	4.171
[5]	0.1671		53.1	62.0	4.171
[6]	0.1671	0.003479	47.9	62.0	0.88
[7]	0.0131		57.5	0.0	4.171
[8]	0.02912	0	29.7	0.0	4.171
[9]	0.02912	0.04133	5.1	0.0	0.88
[10]	0.02912	1	5.1	0.0	0.88
[11]	0.108	0	57.5	52.8	4.171
[12]	0.108		57.5	52.8	64.29
[13]	0.108		90.2	52.8	64.29
[14]	0.09202	0	144.8	62.0	64.29
[15]	0.09202		101.2	62.0	64.29
[16]	0.09202	0.01535	78.6	62.0	4.171
[17]	0.01603		122.8	0.0	64.29
[18]	0.01603	0	87.7	0.0	64.29
[19]	0.01603	0.09991	29.7	0.0	4.171
[20]					
[21]	0.253		275.0		
[22]	0.253		80.3		
[23]	1.1		25.0		
[24]	1.1		43.4		
[25]	0.94		25.0		
[26]	0.94		34.2		
[27]	1.98		13.0		
[28]	1.98		4.7		
[29]	2.04		39.2		
[30]	2.04		40.0		
[31]	0.253		54.3		
[32]	2.04		25.0		

Starting at state point 1, the dilute LiBr-water solution—52.8% LiBr—exits the absorber with a temperature of 29.9°C at the chiller's low pressure of 0.88 kPa. The solution is then pumped to the chiller's intermediate pressure of 4.171 kPa at state point 2. As in the previous cases, it is assumed that the process from state point 1 to point 2 is a constant temperature process. In reality, the solution's temperature may increase slightly as a result of the pumping

process; but that temperature increase is assumed negligible in this model. Before entering the low generator, the dilute solution flows through the solution heat exchanger, where it is preheated by the strong solution leaving the low generator. As a result, the temperature of the dilute solution increases from 29.9°C at state point 2 to 47.3°C at state point 3, a temperature increase of 17.4°C. Simultaneously, the temperature of the strong solution—62.0% LiBr—exiting the low generator decreases from 76.4°C at state point 4 to 53.1°C at state point 5, a temperature decrease of 23.3°C. The preheated dilute solution enters the low generator, in which the addition of heat from the high condenser causes a portion of the water in the solution to vaporize and pass from the low generator to the low condenser. The processes that the refrigerant water experiences after it exits the low generator and enters the refrigerant loop of the bottom half of the integrated double-effect chiller are the same as in the refrigerant loop of the integrated single-effect chiller of Case 2a.

A portion of the LiBr-water solution—52.8% LiBr—exits the low generator and enters the solution loop of the top half of the chiller, while another portion of the solution—62.0% LiBr—exits the low generator and continues through the solution heat exchanger and solution expansion valve in the solution loop of the bottom half of the chiller. The solution that enters the top half of the solution loop at state point 11 with a temperature of 57.5°C and system intermediate pressure of 4.171 kPa is pumped to the system's high pressure of 64.29 kPa at state point 12. Before entering the high generator, it flows through the second solution heat exchanger where it is heated by the strong solution leaving the high generator, resulting in a temperature increase of 32.7°C between state points 12 and 13.

In the high generator, the portion of the microturbine exhaust gas heat—52.45 kW at 275 ^{o}C—that drives the double-effect chiller cycle is input between state points 21 and 22, and the portion of the exhaust gas heat that is used to augment hot water production is input between state points 22 and 31. The dilute solution at state point 13 enters the high generator, where the exhaust gas heat input vaporizes a portion of the water in the solution. This water vapor enters the top half refrigerant loop with a temperature of 122.8°C at the chiller's high pressure, while the concentrated solution—62.0% LiBr—exits the high generator at a

temperature of 144.8°C. By comparing the temperature of the strong solution (143.6°C) at the generator exit in Case 2c with the temperature of the strong solution (144.8°C) at the exit of the high generator in this case, the ability of the double-effect chiller to more efficiently utilize the high temperature microturbine exhaust heat is apparent.

One noticeable difference between the integrated single-effect chiller in Case 2a and the integrated double-effect chiller in this case is the split in the absorber cooling water stream. The split stream design is employed here to increase the temperature of the hot water at the outlet of the generator. If a single stream design with the mass flow rate of 2.04 kg/s—as it is as state point 32 before the split, the temperature change that the cooling water undergoes as it passes through the absorber would decrease, according to a First Law energy balance; and the subsequent temperature increase through the low condenser would be less than it is with the split stream design. Thus, the resulting temperature of the hot water stream would decrease. By utilizing a split stream design, the temperature change of the water in the two cooling streams is maximized, while still providing the required cooling to the absorber and the low condenser.

Table 3.14 lists the net heat transfer rates in the different ACS components for Case 3a. The COP of the chiller in this case is 1.324. Q_{cg} is the internal heat transfer from the low condenser to the low generator.

Table 3.14 Net heat transfer rates in absorption chiller components for Case 3a

Component	Variable	Net Heat Transfer Rate (kW)
Generator	Q_g	**52.45**
Absorber	Q_a	**85.52**
Low Condenser	Q_c	**36.41**
High Condenser/Low Generator	Q_{cg}	**37.79**
Evaporator	Q_e	**69.47 (19.75 RT)**

3.14 Case 3b: Integrated Double-Effect ACS, 122.2 kW Fuel Input, Q_g=64.1kW

Case 3b is derived from Case 3a by scaling up the mass flow rates of Case 3a to account for the actual rated fuel input of 122.2 kW. The result is that the net energy transferred into or out of the absorption chiller's components is also scaled up. The integrated chiller in Figure 3.15 is the chiller in this case. Table 3.15 contains the net heat transfer rates in the different ACS components for Case 3b. The COP of the chiller in this case is 1.324, the same as in Case 3a, because Q_g and Q_e scaled up proportionally.

Table 3.15 Net heat transfer rates in absorption chiller components for Case 3b

Component	Variable	Net Heat Transfer Rate (kW)
Generator	Q_g	64.09
Absorber	Q_a	104.51
Condenser	Q_c	44.49
Low Condenser/Low Generator	Q_{cg}	46.18
Evaporator	Q_e	84.89 (24.14 RT)

3.15 Case 3c: Integrated Double-Effect ACS, 100 kW Fuel Input, Q_g=59.45kW

Case 3c is very similar to Case 3a, except that no portion of the microturbine's exhaust energy is used to augment hot water production. Instead, all of the exhaust energy is used to drive the absorption chiller cycle. The result is an increase in the chilling capacity, Q_e, of the ACS. Table 3.16 contains the EES array of state point results for this case, and Table 3.17 contains the net heat transfer rates in the different ACS components for this case. The COP of the chiller is 1.324, the same as in Case 3a and Case 3b. Because no portion of the microturbine exhaust is used in augmenting hot water production, the temperatures of the exhaust at state point 22 and 31 are equal. Also, it is interesting to note that, even without augmenting the hot water production with exhaust energy, the temperature of the produced hot water is 1°F higher than it is in Case 3a, in which 7.0 kW of the microturbine exhaust is used to produce hot water. The reason that the hot water's temperature is higher in this case than in Case 3a is that the heat rejected from the absorber and low condenser to the hot water production line in this

case is higher by approximately 16 kW. Still, the generator's heat exchanger will be constructed such that the user can allocate a portion of the microturbine exhaust to hot water production, should the applications require various distributions between hot water and space cooling.

Table 3.16 EES array of state point results for Case 3a

	1 m_i [kg/s]	2 q_i [Vapor Quality]	3 T_i [deg C]	4 x_i [LiBr wt. %]	5 P_i [kPa]
[1]	0.2223	0	29.9	52.8	0.88
[2]	0.2223		29.9	52.8	4.171
[3]	0.2223		47.3	52.8	4.171
[4]	0.1893	0	76.4	62.0	4.171
[5]	0.1893		53.1	62.0	4.171
[6]	0.1893	0.003479	47.9	62.0	0.88
[7]	0.01484		57.5	0.0	4.171
[8]	0.033	0	29.7	0.0	4.171
[9]	0.033	0.04133	5.1	0.0	0.88
[10]	0.033	1	5.1	0.0	0.88
[11]	0.1224	0	57.5	52.8	4.171
[12]	0.1224		57.5	52.8	64.29
[13]	0.1224		90.2	52.8	64.29
[14]	0.1043	0	144.8	62.0	64.29
[15]	0.1043		101.2	62.0	64.29
[16]	0.1043	0.01535	78.6	62.0	4.171
[17]	0.01816		122.8	0.0	64.29
[18]	0.01816	0	87.7	0.0	64.29
[19]	0.01816	0.09991	29.7	0.0	4.171
[20]					
[21]	0.253		275.0		
[22]	0.253		54.4		
[23]	1.1		25.0		
[24]	1.1		45.9		
[25]	0.94		25.0		
[26]	0.94		35.4		
[27]	1.98		13.0		
[28]	1.98		3.6		
[29]	2.04		41.0		
[30]	2.04		41.0		
[31]	0.253		54.4		
[32]	2.04		25.0		

Table 3.17 Net heat transfer rates in absorption chiller components for Case 3c

Component	Variable	Net Heat Transfer Rate (kW)
Generator	Q_g	59.45
Absorber	Q_a	96.90
Low Condenser	Q_c	41.25
High Condenser/Low Generator	Q_{cg}	42.82
Evaporator	Q_e	78.72 (22.38 RT)

3.16 Summary of Cases

Table 3.18 contains a summary of the different EES case studies. Included in the table are the configuration of the system; the fuel input basis of the case; the driving heat input to the generator of the absorption chiller (Q_g); the cooling capacity of the chiller (Q_e) in kilowatts and refrigeration tons for the respective driving input and configuration; the coefficient of performance of the chiller—the ratio of Q_e to Q_g; and the heat transfer rate out of the absorber and condenser, Q_a and Q_c, respectively. Additionally, for the integrated chiller configuration, the table lists the amount of microturbine exhaust heat that is dedicated to producing hot water in the generator's integrated heat recovery unit. As noted previously, Cases 1b, 2b, and 3b are scaled up to the Capstone rated fuel input of 122.2 kW (HHV) from Cases 1a, 2a, and 3a, respectively. These cases are provided as a representation of the actual operating conditions based on Capstone's specification, while the 100.0 kW (HHV) fuel input cases are provided for convenient comparison.

Upon comparison of the single-effect chiller cases, Case 2c yields the highest COP—i.e., the greatest chilling capacity for the given driving heat input. However, as discussed before, Case 2c contains certain anomalies and issues that make it purely theoretical, but it provides useful information of the design limit. In actual operation, the results of Case 2a may be more reliable. The absorption chiller configuration of the chiller in Case 2a appears to be preferable to that of the chiller in Case 1a when comparing the chilling capacity of the two chillers. In Case 2a, because the heat recovery unit has been integrated into the absorption chiller's generator, the inefficiency of using a standalone HRU has been mitigated. The result is that more of the microturbine's exhaust energy (52.45 kW versus 47.5 kW) can be used to drive the absorption

cycle. Therefore, the cooling capacity of the chiller increases from 9.73 RT in Case 1a to 10.75 RT in Case 2a. Despite this increase in cooling capacity, using the integrated double-effect absorption chiller in Case 3c yields the highest chilling capacity and COP for 100.0 kW (HHV) fuel input. Depending on the needs of the user and application in terms of hot water production desired, cooling capacity desired, and cost and size limitations, the integrated double-effect chiller in Case 3c appears to be the most robust and efficient configuration.

Table 3.18 Summary of EES Absorption Chiller Case Study Results

Case	ACS Configuration	Fuel Input, kW (HHV)	Q_g (kW)	Q_e (kW/RT)	COP	Q_a (kW)	Q_c (kW)	Q_{hw} (kW)
1a	Standalone / Single-Effect	100.0	47.50	34.23 / 9.73	0.7206	45.45	36.29	N/A
1b	Standalone / Single-Effect	122.2	58.05	41.80 / 11.89	0.7206	55.55	44.35	N/A
2a	Integrated / Single-Effect	100.0	52.45	37.79 / 10.75	0.7206	50.18	40.06	7.00
2b	Integrated / Single-Effect	122.2	64.09	46.18 / 13.13	0.7206	61.32	48.95	8.55
2c	Integrated / Single-Effect	100.0	59.45	46.61 / 13.25	0.784	56.66	49.40	0
3a	Integrated / Double-Effect	100.0	52.45	69.47 / 19.75	1.324	85.52	36.41	7.00
3b	Integrated / Double-Effect	122.2	64.09	84.89 / 24.14	1.324	104.51	44.49	8.55
3c	Integrated / Double-Effect	100.0	59.45	78.72 / 22.38	1.324	96.90	41.25	0

CHAPTER 4

CONCLUSION

This study lays the groundwork for future research in micro-CCHP applications utilizing the novel, integrated single-effect and double-effect water-lithium bromide absorption chiller presented in Chapter 3. It provides a launching point for future research through the following contributions:

1. The study models a new single-effect and double-effect absorption chiller that integrates the heat recovery unit into the chiller's generator, eliminates the need for a cooling tower by integrating its function into the chiller through the modification of internal piping, and uses energy in the chiller that would otherwise be wasted to the environment through the inefficiency of a standalone HRU or through the rejection of heat to a cooling tower and absorber. Through the development of a system of equations and the utilization of Engineering Equation Solver as a tool to provide a useful and in depth understanding of these novel integrated chillers, the details of every state point inside the chiller—temperature, pressure, concentration, fluid properties—are now understood. These details have come to light as a result of this study, and they have been employed to validate the efficacy of the design of the integrated chillers and to complete the heat and material balances of the overall micro-CCHP system designs. It has been verified that there exists a sufficiently large temperature difference (ΔT) between the microturbine exhaust gas that drives the absorption cycle and the solution inside the generator. This indicates that the integration of the HRU inside the generator will entail a more compact heat exchanger, the design of which may form the basis for future research.

2. By modifying the EES model developed in this study and applying its results to the overall micro-CCHP system model, the integrated absorption chillers have been scaled up from 100 kW to the rated fuel input, 122.2 kW (HHV), of the

Capstone C30 gas microturbine. This practice paves the road for further scaling up to much larger systems in the future.

3. In the exploratory study of Case 2c, a possible means of reducing the refrigerant flow rate and, thus, the size of the absorption chiller, while still maintaining a standard of performance, was discovered. This case may also provide the grounds for future research into making a more compact integrated chiller, reducing the footprint of the overall system.

4. Finally, this study shows the possibility of achieving high levels of system thermal performance. While the performance of existing systems is capped at around 70%, the use of the integrated single-effect and double-effect chillers presented herein provides a means of increasing performance. The single-effect integrated chiller enhances the performance of its associated micro-CCHP system, which yields 22.9 kW of electricity, a 1.6 kW electricity enhancement from cooling the inlet of the gas microturbine, 92.2 kW of hot water, and 34.8 kW of chilled water for every 100 kW (HHV) of fuel input. The enhanced performance of this system is 151.5%. The double-effect integrated chiller further enhances the performance of its associated system by producing, for every 100 kW (HHV) of fuel input, 22.9 kW of electricity, a 1.6 kW electricity enhancement from turbine inlet cooling, 123.9 kW of hot water, and 66.47 kW of chilled water. The enhanced performance of this system is 214.9%. This performance shows that the system's output of useful energy products more than doubles the fuel input of 100 kW (HHV); and from the prospect of achieving such a high system performance comes the inspiration for future research into this system and, with it, the potential for a new breed of high performance micro-CCHP systems.

REFERENCES

Angrisani, G., Roselli, C., Sasso, M. "Distributed Microtrigeneration Systems." *Progress in Energy and Combustion Science* 38 (2012): 502-521.

ASHRAE Handbook 2001 Fundamentals. American Society of Heating, Refrigerating, and Air-Conditioning Engineers, Inc. New York, New York: 2001.

ASHRAE Handbook 2010 Refrigeration. American Society of Heating, Refrigerating, and Air-Conditioning Engineers, Inc. New York, New York: 2010.

Capstone Turbine Corporation. *Capstone MicroTurbine: Capstone C30 Low Pressure Natural Gas*. Commercial brochure, 2002. Web. 17 November 2011. < http://www.microturbine.com>.

Capstone Turbine Corporation. *Capstone MicroTurbine Model C30 User's Manual* (Rev A). 2012. Web. 17 November 2011. < http://216.163.110.250/dls/1.pdf>.

Dorgan, C.B., Leight, S.P., Dorgan, C.E. *Application Guide for Absorption Cooling/Refrigeration Using Recovered Heat*. Atlanta, GA: ASHRAE, 1995.

Energy Solutions Center, Inc. "The Energy Solutions Center DG Applications Guide." 2012. Web. 10 October 2013. < http://www.understandingchp.com/AppGuide/Chapters/Chap4/4-1_Recip_Engines.htm>.

Figueredo, G.R., Bourouis, M., Coronas, A. "Thermodynamic Modelling [sic.] of a Two-Stage Absorption Chiller Driven at Two-Temperature Levels." *Applied Thermal Engineering* 28 (2008): 211-217.

Herold, K.E., Radermacher, R., Klein, S.A. *Absorption Chillers and Heat Pumps*. Boca Raton, FL: CRC Press, 1996.

Johnson Controls, Inc. *York by Johnson Controls: YIA Single-Effect Absorption Chillers Steam And Hot Water Chillers*. 2010. Web. 15 February 2012. <http://www.johnsoncontrols.com>.

Khemani, Haresh. "Ammonia-Water Vapor Absorption Refrigeration System." Ed. Lamar Stonecypher. *Bright Hub Engineering*, 2010. Web. 15 October 2013. <http://brighthubengineering.com>.

Mohanty, B., Paloso, G. "Enhancing Gas Turbine Performance by Intake Air Cooling Using an Absorption Chiller." *Heat Recovery Systems & CHP* 15-1 (1995): 41-50.

Puig-Arnavat, M., Lopez-Villada, J., Bruno, J.C., Coronas, A. “Analysis and Parameter Identification for Characteristic Equations of Single- and Double-Effect Absorption Chillers by Means of Multivariable Regression.” *International Journal of Refrigeration* 33 (2010): 70-78.

Somers, C. *Simulation of Absorption Cycles for Integration into Refining Processes*. Thesis, University of Maryland. College Park, MD: 2009.

U.S. DOE Gulf Coast Clean Energy Application Center. “BP Helios Plaza Project Profile.” Web. 29 May 2012. <http://gulfcoastcleanenergy.org/ProjectProfiles/tabid/1636/Default.aspx >.

U.S. DOE Gulf Coast Clean Energy Application Center. “Targa Resources Project Profile.” Web. 29 May 2012. <http://gulfcoastcleanenergy.org/ProjectProfiles/tabid/1636/Default.aspx >.

Uzuneanu, K., Scarpete, D. “Energetic and Environmental Analysis of a Micro CCHP System for Domestic Use.” *6th IASME / WSEAS International Conference on Energy & Environment (EE ’11)*, Cambridge, UK: 2011.

Wang, T., Braquet, L. “Assessment of Inlet Cooling to Enhance Output of a Fleet of Gas Turbines.” *Proceedings of Industrial Energy Technology Conference IETC 30th*, New Orleans, LA: 2008.

Wang, X., Chua, H.T. “Absorption Cooling: A Review of Lithium Bromide-Water Chiller Technologies.” *Recent Patents on Mechanical Engineering* 2 (2009): 193-213.

Wu, D.W., Wang, R.Z. “Combined Cooling, Heating and Power: A Review.” *Progress in Energy and Combustion Science* 32 (2006): 459-495.

Yazaki Energy Systems, Inc. *Water Fired Chiller/Chiller-Heater: WFC-S Series*. Commercial brochure, SB-WFCS-1009. Web. 5 December 2011. <http://www.yazakienergy.com>.

Yin, Hongxi. *An Absorption Chiller in Micro BCHP Application: Model Based Design and Performance Analysis*. Dissertation, Carnegie Mellon University. Pittsburgh, PA: 2006.

Yin, H., Qu, M., Archer, D.H. “Model Based Experimental Performance Analysis of a Microscale LiBr-H_2O Steam-Driven Double-Effect Absorption Chiller.” *Applied Thermal Engineering* 30 (2010): 1741-1750.

APPENDIX A

COMPANY PROFILES

Turbines

Company name: Capstone Turbine Corporation

Address: 21211 Nordhoff Street

Chatsworth, CA 91311

Phone: 1 866 4 CAPSTONE
1 818 734 5300

Email: ir@capstoneturbine.com (investor relations)

URL: http://www.capstoneturbine.com/

Summary: Capstone Turbine Corporation produces microturbines ranging from 30 kW to 200 kW for a variety of applications. Capstone also produces larger turbines up to 10 MW. Their turbines can operate on low or high pressure natural gas, biogas, flare gas, diesel, propane, or kerosene. Capstone turbines are the most commonly used turbines for Micro-CHP and CCHP applications.

Company name: Micro Turbine Technology BV

Address: De Rondom 1
Eindhoven
5612 AP
The Netherlands

Phone: +31 (0)88 688 0000

Email: info@mtt-eu.com

URL: http://www.mtt-eu.com/

Summary: MTT offers a 3 kW microturbine marketed for CHP applications. The company claims that this turbine achieves 16% electrical efficiency, which they say is a world record for a turbine of this size. In addition to their 3 kW turbine, MTT is also currently developing a 30 kW microturbine.

Absorption Chillers

Company name: Thermax (USA)

Address: 21800 Haggerty Road, Suite 112
Northville, MI 48167

Phone: (248)468-0541

Email: Piyush Patel, Absorption Product Manager
ppatel@thermax-usa.com Cell: 248 756 5398

URL: http://www.thermax-usa.com/

Summary: Thermax has several divisions worldwide that specialize in solutions, such as cooling and heating, power generation, air purification, water and sewerage treatment, and specialty chemicals. Its Cooling and Heating division offers a variety of single and double effect absorption chillers both water/Lithium bromide and Ammonia/water ranging in cooling capacity from 10 TR to 4000 TR depending on the application. Thermax's absorption chillers can be driven by steam, hot water, gas/liquid fuels, exhaust gases, or a combination of these. The company considers the strength of its Cooling and Heating division to be customized solutions that meet the needs of the individual customer. Thermax operates out of the USA, China, India, and the UK, with its subsidiary Thermax Cooling and Heating Eng. Company Limited in Zhejiang, China.

Company name: Yazaki Energy Systems, Inc.

Address: 701 E. Plano Parkway, Suite 305
Plano, TX 75074-6700

Phone: (469) 229-5443

Email: yazaki@yazakienergy.com

URL: http://www.yazakienergy.com/

Summary: Yazaki Energy Systems, Inc., offers gas-fired double effect and water-fired single effect water/Lithium bromide absorption chillers ranging in cooling capacity from 10 TR to 200 TR. The company's offices are located

primarily in the United States, but it also has offices in Central and South America and in Europe (Italy and Germany).

Company name: York by Johnson Controls

Address: 5757 N. Green Bay Ave.
P.O. Box 591
Milwaukee, WI 53201

Phone: (414)524-1200

Email: systems-uk.cg-eur@jci.com

URL: http://www.johnsoncontrols.co.uk

Summary: York offers hot water, steam, and direct-fired single effect and double effect water/Lithium bromide absorption chillers that range in cooling capacity from 80 TR to 900 TR.

Company name: Trane

Address: 530 Elmwood Park Blvd.
Harahan, LA USA 70123

Phone: (504)733-6789 (Local Sales Office)

Email: Mike Determann, Equipment Solutions Manager
MDetermann@trane.com

URL: http://www.trane.com/COMMERCIAL/DNA/View.aspx?i=976

Summary: Trane offers single and double effect hot water driven, steam driven, and direct-fired Thermax absorption chillers ranging in cooling capacity from 111 TR to 2029 TR. The company provides installation and service for the Thermax chillers offered.

Company name: Robur Corporation

Address: 827 E. Franklin Street
47711 Evansville, IN

Phone: (812) 424-1800

Email: sales@robur.com

URL: http://www.roburcorp.com/

Summary: Robur Corporation offers single effect gas-fired ammonia/water absorption chillers with or without a heat recovery option. Robur units are 4 TR to 5 TR in cooling capacity without and with heat recovery, respectively. Units can be combined modularly in series to achieve cooling capacities of up to 25 TR. Robur absorption chillers are air-cooled; therefore, no cooling tower is necessary.

Company name: FireChill Ltd.

Address: Round Foundry Media Centre
Foundry St
Leeds
LS11 5QP

Phone: +44 (0) 113 394 4576

Email: john@firechill.com

URL: http://www.firechill.com/

Summary: FireChill Ltd. offers two 5 TR single effect ammonia/water absorption chillers, one that is gas-fired and one that is waste heat and/or direct-fired. Either of the units can be combined modularly into a 2-6 unit multipack that can yield cooling capacities up to 30 TR. Additionally, FireChill has partnered with Capstone to produce the PowerChill, a pre-packaged micro-CCHP system that combines four FireChill absorption chillers with heat recovery capability with a 30 or 65 kW Capstone microturbine.

Company name: Cooling Technologies, Inc.

Address: 333 14th Street

Toledo, OH 43624

Phone: (419)536-9006

Email: info@coolingtechnologies.com

URL: http://www.coolingtechnologies.com/index.htm

Summary: Cooling Technologies, Inc. offers a single effect 5 TR ammonia/water absorption chiller manufactured and distributed by its partner FireChill. The chiller offered by Cooling Technologies, Inc. is air-cooled, is driven by natural gas or propane, and has proprietary heat recovery capability.

Pre-Packaged CHP and CCHP systems

Company name: Integrated CHP Systems Corp.

Address*:* 50 Washington Rd
Princeton Junction, NJ 08550

Phone: (609) 799-2340

Email: gearoid@ichps.com

URL: http://www.ichps.com/

Summary: Integrated CHP Systems Corp. offers a pre-fabricated integrated cooling and heating module (ICHM) designed for cogeneration applications with internal combustion engines. The ICHM includes an absorber, load heat exchanger, cooling tower, condenser pump, system controls, pipe, valves and fittings in an outdoor enclosure.

Company name: Kraft Energy Systems, LLC

Address: 199 Wildwood Avenue

Woburn, MA 01801

Phone: (800)969-6121

(781)938-9100

Email: dbarstow@kraftpower.com

URL: http://www.kraftenergysystems.com/index.html

Summary: Kraft Energy Systems, LLC, a subsidiary of the Kraft Power Corporation, offers pre-packaged combined heating and power systems that range in power supply from 50 kW to 3 MW with overall system efficiencies of up to 89%. The company's CHP systems use IC engines as the prime mover. The systems can run on natural gas, landfill/digester gas, biodiesel, or coal bed methane.

Company name: IPower Energy Systems, LLC

Address: 4640 Dr. Martin Luther King Jr. Blvd.
Anderson, Indiana 46013-2317

Phone: (704)889-5229
(765)621-2977

Email: mhudson@ipoweres.com

dmosbaugh@ipoweres.com

URL: http://www.ipoweres.com

Summary: IPower Energy Systems, LLC, offers pre-packaged CHP systems driven by IC engines that run on either biogas or natural gas. The company offers three biogas-fueled CHP systems with electrical outputs of 20 kW, 65 kW, and 280 kW. The maximum overall system efficiency of the biogas-fueled CHP system is 86.5%. IPower offers three natural gas-fueled CHP systems with electrical outputs of 23 kW, 85 kW, and 365 kW. The maximum overall system efficiency of the natural gas-fueled CHP system (365 kW) is 90.0%.

Company name: Packaged Plant Solutions, Ltd.

Address: Unit 8 Thornton Chase
Linford Wood
Milton Keynes MK14 6FD

Phone: 01908 711371

Email: nfo@packagedplant.com

URL: http://www.packagedplant.com

Summary: Packaged Plant Solutions offers plug and play turbine-driven CHP units that range in electrical output from 24 kW to 2 MW with overall system efficiencies of up to 80%.

APPENDIX B

RESOURCES FOR THE PROPERTIES OF LITHIUM BROMIDE SOLUTIONS

The following papers provide valuable information on the properties of lithium bromide solutions:

Macriss, R.A., Zawacki, T.S., 1989, "Absorption Fluid Data Survey: 1989 Update," ORNL Report, ORNL/Sub84-47989/4.

Patek, J., Klomfar, J. "A Computationally Effective Formulation of the Thermodynamic Properties of LiBr–H_2O Solutions from 273 to 500 K over Full Composition Range." *International Journal of Refrigeration* 29 (2006): 566-578.

Kaita, Y. "Thermodynamic Properties of Lithium Bromide-Water Solutions at High Temperatures." *International Journal of Refrigeration* 24 (2001): 374-39.

ASHRAE Handbook 2001 Fundamentals, ASHRAE, New York, New York.

The figure on the next page, taken from the *2001 ASHRAE Fundamentals Handbook*, is the enthalpy-concentration diagram for water-lihtium bromide solutions

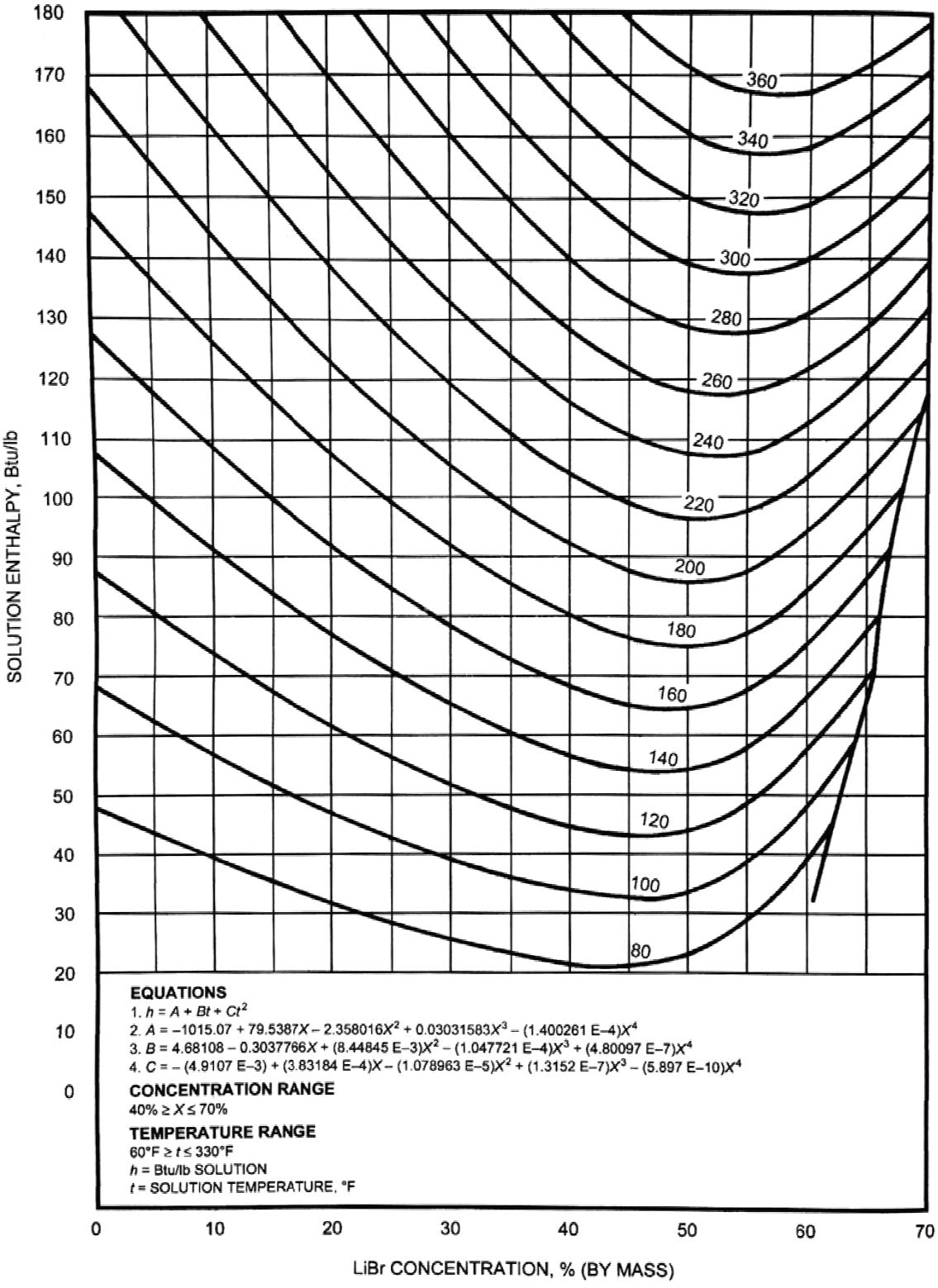

Enthalpy-Concentration Diagram for Water-Lithium Bromide Solutions (Source: ASHRAE Handbook 2001 Fundamentals)

APPENDIX C

ITERATIVE PROCEDURE FOR CALCULATING THE MASS FLOW RATE OF DILUTE WATER-LITHIUM BROMIDE SOLUTION AT STATE POINT 1 IN CASE 2C

The following combination of hand calculations and EES calculations are performed to determine the mass flow rate of the dilute H_2O-LiBr solution at state point 1 in Case 2c.

Starting with the input conditions of Case 2a, increase T[4] to 120°C, and run the EES program. This yields Q_g = 127.2 kW.

Now, use the following proportion to solve for the m[1] that will make Q_g equal to 59.45 kW:

$$\frac{m[1]^*}{Q_g^*} = \frac{m[1]}{59.45kW}, \qquad \text{Eqn. 1a}$$

Where m[1]* is the mass flow rate of the dilute water-LiBr solution at state point 1 (as shown on Figure 3.17 in Chapter 3), Q_g* is the value of Q_g of the current iteration, and m[1] is the dilute solution mass flow rate that will yield a value of Q_g equal to 59.45 kW at the current iteration's value of T[4], the temperature of the strong water-LiBr solution leaving the generator.

Therefore, at the current conditions, $\frac{0.17874kg/s}{127.2kW} = \frac{m[1]}{59.45kW}$, which yields m[1] = 0.0835 kg/s.

Next, as a check, plug m[1] = 0.0835 kg/s into the EES routine and re-run EES to verify that Q_g = 59.45 kW.

Once it is verified that Q_g = 59.45 kW, increase T[4] again. This time, T[4] can be increased to 140°C. Run EES and check Q_g. The new value of Q_g at T[4] = 140°C is 73.43 kW.

Using the proportion in Eqn. 1a again with m[1]* = 0.0835 kg/s and Q_g*=73.43 kW yields m[1]=0.06760 kg/s.

Perform the check step again to verify that Q_g = 59.45 kW. Because of round-off error on m[1], Q_g is sometimes not exactly equal to 59.45 kW; therefore, more decimal places may need to be carried on m[1].

Once it is verified again that Q_g = 59.45 kW, increase T[4] to 150°C now and run EES. This gives an error message that "Iterative calculations in x_LiBr did not converge." This means that, at the current pressure, the empirical property correlations for the concentration of LiBr in the

solution are undefined. For this reason, T[4] must be decreased below 150°C. Several values of T[4] are experimented with between 140°C and 150°C, until the maximum value for which the solution converges is reached. At the current pressure of 7.347 kPa, that maximum value of T[4] for which the solution converges is 143.6°C.

With T[4] = 143.6°C, the EES routine is run to get the corresponding value of Q_g, which is now 61.04 kW.

Finally, using the proportion of Eqn. 1a again with m[1]* = 0.06760 kg/s and Q_g* = 61.04 kW, it is determined that the mass flow rate of the dilute solution exiting the absorber that makes Q_g equal to 59.45 kW is m[1] = 0.065839 kg/s.

VITA

Scott Joseph Richard was born in New Orleans, Louisiana, in 1982. He earned his B.A. in English from the University of New Orleans (UNO) in December 2005, and he began teaching English at Mount Carmel Academy, the all-girls' Catholic high school where he met his wife—a fellow English teacher, in 2006. After two years of teaching modern American literature to seniors, he retired from teaching and began pursuing a degree in Mechanical Engineering. Scott earned his B.S. in Mechanical Engineering from the University of New Orleans in 2011 and started his graduate coursework in Mechanical Engineering the next semester. Scott worked as a Graduate Research Assistant and studied under Dr. Ting Wang at the Energy Conversion and Center at UNO throughout his graduate school career. He earned his Masters of Science in Engineering in December 2013. He currently lives in New Orleans, where he works for a Fortune 500 engineering firm as a Mechanical Engineer in the oil & gas industry.